Citation
Huang, Z. and Chen, W. and Hao, H. and Chen, Z. and Pham, T.M. and Tran, T.T. and Elchalakani, M. 2021. Shear behaviour of ambient cured geopolymer concrete beams reinforced with BFRP bars under static and impact loads. Engineering Structures. 231: ARTN 111730. http://doi.org/10.1016/j.engstruct.2020.111730

Shear Behaviour of Ambient Cured Geopolymer Concrete Beams Reinforced with BFRP Bars under Static and Impact Loads

Zhijie Huang[1,2], Wensu Chen[2*], Hong Hao[2*], Zuyu Chen[1,3], Thong M. Pham[2], Tung T. Tran[2], Mohamed Elchalakani[4]

1. Institute of Geotechnical Engineering, College of Civil Engineering and Architecture, Zhejiang University, Hangzhou 310058, China

2. Center for Infrastructural Monitoring and Protection, School of Civil and Mechanical Engineering, Curtin University, Australia

3. Department of Geotechnical Engineering, China Institute of Water Resources and Hydropower Research, Beijing 100048, China

4. School of Civil, Environmental and Mining Engineering, The University of Western Australia, 35 Stirling Highway, WA 6009, Australia

*Corresponding authors. wensu.chen@curtin.edu.au (W. Chen), hong.hao@curtin.edu.au (H. Hao).

Abstract: The use of fiber reinforced polymer (FRP) bars in GeoPolymer Concrete (GPC) structures has drawn increasing attention in recent years. The application of GPC with basalt fiber reinforced polymer (BFRP) reinforcements in replacing Ordinary Portland cement Concrete (OPC) and steel reinforcements leads to green and sustainable constructions. Currently, very limited studies have been conducted to investigate the performance of GPC beams reinforced with BFRP bars under static loads, but no study on their performance under impact loads has been reported yet in open literature. In this study, ambient-cured GPC beams reinforced with BFRP bars were designed, cast and tested under static and impact loads. The damage mode and quantitative results such as midspan deflection, reinforcement strain, and impact and reaction forces were recorded and analysed. Test results showed that spiral stirrups led to superior performance of the beams under both static and impact loads as compared to conventional rectangular stirrups. The commonly used concrete material model *Mat_072R3 in LS-DYNA was modified based on test data to model GPC material. With the modified GPC material model, numerical models were developed and calibrated against the impact test results. Parametric studies were carried out to investigate the influences of GPC material strength and longitudinal and stirrup reinforcement ratios on the performance of beams subjected to impact loads. It was also found that

using steel bars as the compression reinforcements led to better performance because BFRP bars under shear and compression were vulnerable to splitting damage subjected to impact loads.

Keywords: Geopolymer Concrete beam; BFRP bar; Shear; Static test; Impact test; Numerical simulation

1. Introduction

Reinforced Concrete (RC) structures, usually composed of Ordinary Portland cement Concrete (OPC) and steel reinforcements, are widely used in construction of buildings, roads, bridges, tunnels, and other civil infrastructures. The demand for OPC and steel reinforcements is expected to increase in the future due to the rising needs of infrastructure in many developing countries, which will cause tremendous amounts of carbon dioxide (CO_2) emissions [1] as a result of the energy-intensive process of producing cement and steel reinforcements. On the other hand, corrosion of steel reinforcement imposes threat to the built RC structures. Corrosion induced damage causes deterioration of RC structures. Even worse, it could result in catastrophic collapse of RC structures in extreme situations. Therefore, maintenance cost is high for retrofitting and repairing the corrosion damaged RC structures, especially those in aggressive and corrosive environments such as marine and coastal areas.

Currently, alternative materials for OPC and steel reinforcements are explored to reduce CO_2 emission and mitigate corrosion issue in RC structures, respectively. GeoPolymer Concrete (GPC) is considered as a sustainable material and a promising replacement for OPC since it utilizes industrial wastes as binders, e.g., fly ash and slag [2]. Reuse of these industrial wastes is of great benefit to environmental sustainability. Except these industrial wastes, construction and demolition wastes such as red clay bricks [3] and ceramic tile wastes [4] can also be used as raw materials of binders. In addition, GPC has good resistance to fire, acid, and sulphate attack, and can be designed and mixed to reach a high compressive strength [5], which has gained increasing attention in recent years [6-8]. On the other hand, fiber reinforced polymer (FRP) reinforcements become a popular alternative to steel reinforcements due to the advantages of high tensile strength, lightweight, high fatigue endurance, and good corrosion resistance [9]. The application of GPC with FRP reinforcements has drawn great attention in recent years [10, 11].

Over the past decades, many studies have been conducted to investigate the shear performance of OPC beams reinforced with FRP bars under static loads [12-17]. Standards such as CSA S806 [18] and ACI 440.1R [19] were also developed to guide the design of OPC beams reinforced with FRP bars. However, very limited studies have been carried out to investigate the shear performance of GPC beams reinforced with FRP bars under static loads. Maranan et al. [10, 20] conducted experiments to investigate the effects of stirrup type, stirrup spacing, tension reinforcement ratio, and shear span-to-effective depth ratio on the shear behaviour of GPC beams reinforced with glass fiber reinforced polymer (GFRP) bars. Test results showed that the beams reinforced with rectangular GFRP stirrups had a similar shear resistance as compared to those reinforced with steel stirrups while they had lower shear strength as compared to those reinforced with spiral GFRP stirrups. Decreasing the spacing of rectangular GFRP stirrups from 150 mm to 75 mm for short beams with a shear span-to-effective depth ratio of 1.8 had no significant effect on the shear capacity of the beams, whereas decreasing the spacing of spiral GFRP stirrups from 150 mm to 75 mm for slender beams with a shear span-to-effective depth ratio of 3 could lead to a higher shear resistance of the beams. Test results also showed that increasing the tensile reinforcement ratio and decreasing the shear span-to-effective depth ratio could increase the shear capacity of the beams due to the increased flexural stiffness and the increased arch action, respectively [21].

With the possible terrorist attacks, accidental explosions, vehicle crash, and falling object impact, the performance of structures subjected to impact loads has received great attentions. There are limited studies on the flexural behaviour of statically flexure-critical OPC beams reinforced with FRP bars under impact loads. Goldston et al. [22, 23] investigated the influences of concrete strength, tension reinforcement ratio, and drop height on the impact behaviour of OPC beams reinforced with GFRP bars in drop weight tests. It was found that higher concrete compressive strength and reinforcement ratio could result in lower maximum midspan deflection of the beams. With increase in drop height, the beams exhibited the failure mode from concrete crushing on the top to the rupture of tension reinforcements. The dynamic amplification factor (DAF) of 1.15-1.17 was obtained by calculating the ratio of dynamic moment capacity to static moment capacity. Based on the tested beams in [22], Saleh et al. [24] built a numerical model and calibrated it against the test results. Parametric studies showed that given similar initial kinetic energy of the drop weight, higher impact velocity could lead to higher impact and reaction forces but lower midspan deflection while the crack pattern changed from flexure-dominant to shear-dominant. Saleh et al. [25, 26] also conducted impact tests to investigate the influences of stirrup spacing and dropping height on the behaviour of GFRP reinforced OPC beams. Test results showed that decreasing the stirrup spacing led to smaller residual deflection and higher residual capacity of the beams and resulted in the failure shifting from shear-plug mode to flexure-shear combined or flexure-governed mode. With the increased dropping height, all the beams experienced severer local damage and wider post-impact cracks.

Currently, no study can be found in open literature on the shear behaviour of statically shear-critical GPC beams reinforced with FRP bars under impact loads. Since GPC and OPC have different material properties such as brittleness and post-failure behaviour under compression [27, 28], the shear performance of GPC beams reinforced with FRP bars under impact loads might be different from those of OPC beams. In this study, five ambient-cured GPC beams reinforced with BFRP bars were prepared. Three beams were tested under static loads while the other two beams were tested under impact loads. The responses of the beams were investigated and analysed in terms of failure mode, crack pattern, load-deflection curve, reinforcement strain, and impact and reaction forces. In addition, concrete material model *Mat_072R3 (KCC model) in LS-DYNA was modified and calibrated based on GPC material test data. With the modified concrete material model, numerical models were developed and calibrated against impact test results of GPC beams reinforced with BFRP bars. Parametric studies were then performed to investigate the effects of GPC compressive strength, tension reinforcement ratio, stirrup ratio, and compression reinforcement type on the performance of the beam under impact loads.

2. Test program

2.1. Materials

2.1.1 Geopolymer concrete

The mix design of the ambient-cured GPC used in this study was developed based on the previous studies [29-31] and given in **Table 1** to achieve a compressive strength of about 40 MPa. Two commercially available source materials, i.e., fly ash and slag, were used in the study. The alkaline solution was a combination of 12 M sodium hydroxide (NaOH) and D-grade sodium silicate (Na_2SiO_3) solution. Crushed stones with the maximum sizes of 7 mm and 10 mm were used as coarse aggregates and silica sand was used as fine aggregates. Six cylinders with a dimension of 100 mm × 200 mm were also cast corresponding to each prepared GPC beam to determine the GPC compressive strength. After casting, all the GPC beam specimens and cylinders were cured under ambient condition in the lab.

Table 1 Mix design of GPC (kg/m^3)

Coarse aggregates		Fine aggregates	Binder		Solution		Solution /binder ratio
Size 7 mm	Size 10 mm	Silica sand	Fly ash	Slag	Na_2SiO_3	NaOH	
598	598	644	360	40	173.7	59.4	0.6

2.1.2 BFRP bars

The basalt fiber reinforced polymer (BFRP) bars consisted of basalt fibers (reinforcing material) embedded into a matrix, i.e. epoxy resin. The epoxy resin encapsulated the fibers to transfer stress and provide protection while the fibers provided stiffness and strength to the composite. In this study, 16-mm-diameter straight bars were used as longitudinal reinforcements, 4-mm-diameter conventional rectangular stirrups and 4-mm-diameter spiral stirrups were employed as transverse reinforcements as shown in **Fig. 1**. The specified tensile strength f_{fu}, modulus of elasticity E_f, and elongation ε_{fu} of these reinforcements were 1200 MPa, 55 GPa, and 0.02, respectively, provided by the manufacturer [32].

(a)

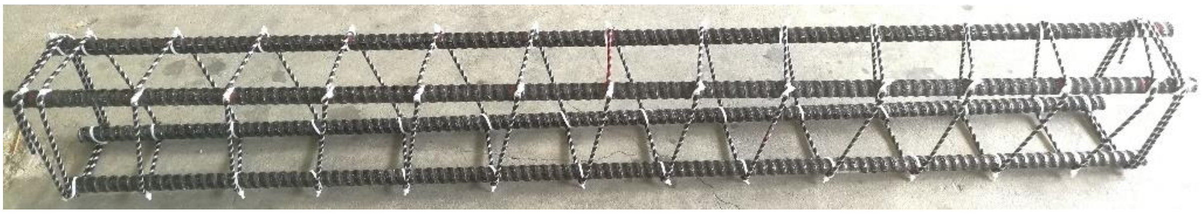

(b)

Fig. 1. BFRP cages for GPC beam casting: (a) rectangular stirrups and (b) spiral stirrups

2.2. Test specimens

A total of five GPC beams were designed and prepared. Three beams were tested under static loads (three point bending) while the other two beams were prepared for drop hammer impact test. The beams had the dimensions of width (b) of 150 mm, depth (h) of 200 mm, and length (L_t) of 1250 mm. **Fig. 2** shows the details of the beam geometry and the reinforcements. The concrete cover (c) of the beams was 20 mm and the effective depth (d) was 168 mm. To investigate the shear behaviour of GPC beams reinforced with BFRP bars, the beams were designed with their flexural capacities (i.e. 100 kN) about twice of the shear capacities (i.e. 45 kN), indicating that all the beams are prone to fail in shear under static loads. Since no standard is available for the design of FRP bars reinforced GPC beams, the beam design in this study was based on Standard ACI 440.1R-15 [19], which is used for FRP bars reinforced OPC beams.

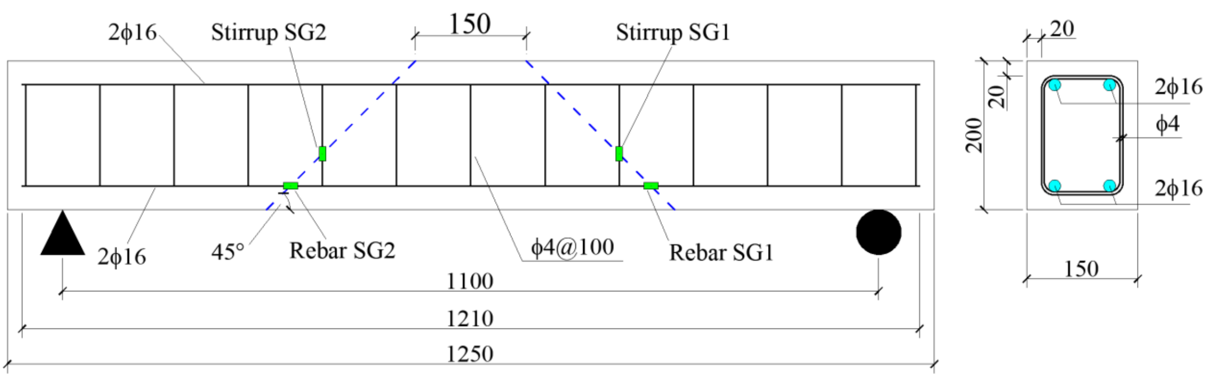

(a)

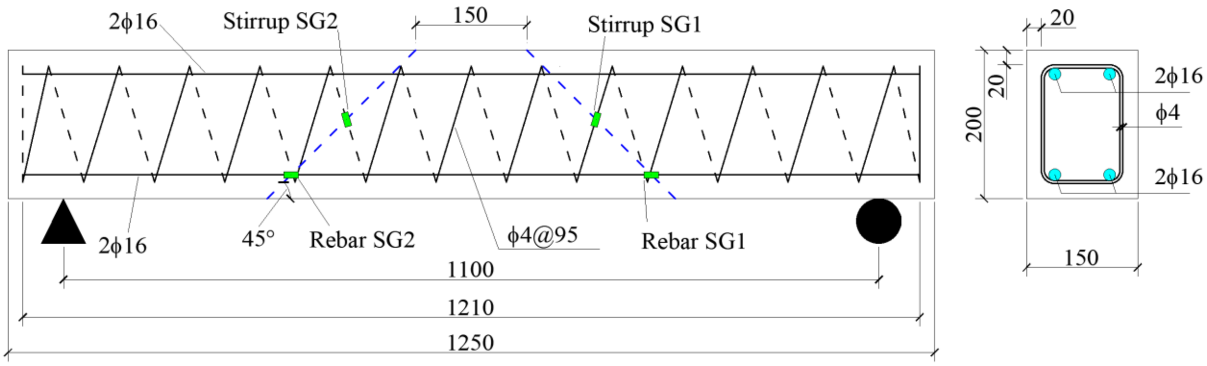

(b)

Fig. 2. Configuration of the tested beams with (a) rectangular stirrups and (b) spiral stirrups

Table 2 gives the details of the tested beams. For easy reference, the beam labels include four parts: the first part represents the concrete type, i.e., GPC; the second part with the letters of "S" and "I" denotes the load conditions, namely, static loads and impact loads, respectively; the third part is the stirrup type, i.e., no stirrup (NS), conventional rectangular stirrup (RS), and spiral stirrup (SP); the last number is concrete compressive strength f_c'. For instance, Beam GPC-I-RS-47 means the beam with the concrete strength of 47 MPa was transversely reinforced with conventional rectangular stirrups and tested under impact loads. The first beam (GPC-S-NS-34) was designed without stirrups to determine the shear contribution of GPC to the beam capacity under static loads. The second beam (GPC-S-RS-52) was transversely reinforced with conventional rectangular stirrups to determine the shear contribution of stirrups to the beam capacity under static loads. Meanwhile, it was a reference beam for impact tests. The third beam (GPC-S-SP-40) was transversely reinforced with continuous spiral stirrups and designed having the same stirrup ratio and similar shear capacity as the second beam (GPC-S-RS-52) to investigate the effect of stirrup type on the shear behaviour of the beam under static loads. The fourth beam (GPC-I-RS-47) was similar to the second beam (GPC-S-RS-52) to investigate the shear behaviour of the beam under impact loads. The fifth beam (GPC-I-SP-46) was similar to the third beam (GPC-S-SP-40) to investigate the effect of stirrup type on the impact behaviour of the beam. It is worth noting that the five prepared beams have different GPC strengths because they were mixed and cast separately owing to the small capacity of the mixer in the lab.

Table 2 Details of the tested beams

Beam	Concrete type	Load condition	Stirrup type	Compressive strength f_c' (MPa)	Stirrup ratio ρ_{fv} (%)	Designed shear capacity (kN)	Designed flexural capacity (kN)
GPC-S-NS-34	GPC	Static	No stirrup	34	0	44.8	90.4
GPC-S-RS-52	GPC	Static	Rectangular	52	0.17	48.1	107.8
GPC-S-SP-40	GPC	Static	Spiral	40	0.17	46.0	97.4
GPC-I-RS-47	GPC	Impact	Rectangular	47	0.17	47.3	104.0
GPC-I-SP-46	GPC	Impact	Spiral	46	0.17	47.1	103.2

2.3. Testing program and instrumentation

2.3.1 Quasi-static test setup

Fig. 3 shows the quasi-static test setup. The beams were simply supported by a pin and a roller in a three-point bending condition with a clear span (L) of 1100 mm. The load was applied by a hydraulic jack at a rate about 3 mm/min. A load cell and linear variable differential transformers (LVDTs) were used to record the applied loads and the corresponding midspan deflection of the beams, respectively. Four strain gauges (SGs) were attached to the bottom longitudinal bars (tension reinforcements) and stirrups at an angle of 45° initiated from the load point as shown in **Fig. 2**. The shear behaviour of the tested beams under static loads, i.e., crack pattern, failure mode, shear capacity, load-midspan deflection relation, load-strain relation of the reinforcements were investigated. Meanwhile, the test results were compared with the predicted results based on Standards ACI 440.1R-15 [19] and CSA S806-12 [18].

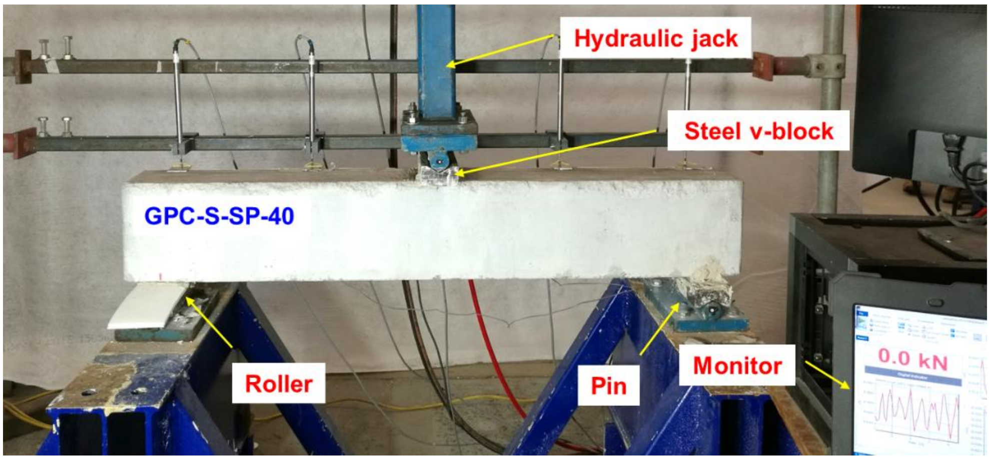

Fig. 3. Quasi-static test setup

2.3.2 Impact test setup

Drop-weight impact tests, widely used to investigate the impact behaviour of concrete beams [33-35], were carried out by dropping a hammer from a certain height onto the midspan of the beams using the impact test setup as shown in **Fig. 4**. The beams had a clear span (*L*) of 1100 mm, which was the same as static test. Two load cells were fixed onto the top and the bottom of the left support to record the reaction forces. Another load cell was placed on the midspan of the beams to measure the impact forces. This load cell was attached to a load cell adaptor with the dimension of 150 mm × 200 mm × 20 mm. In order to produce an even contact surface, plaster was used between the beam surface and the load cell adaptor. Four strain gauges (SGs), the same as static test, were bonded onto the bottom longitudinal bars and stirrups as shown in **Fig. 2**. The hammer with the weight of 203.5 kg was dropped from 2 m height for all the beams. More details about the impact test apparatus could be referred to reference [35]. Impact velocity of the drop hammer, failure progress and midspan deflection of the tested beams were captured by a high speed camera with the rate of 20,000 frames per second. A data acquisition system was used to record the impact force and reinforcements strain with the frequency of 50 kHz. The results of the impact tests such as crack pattern, failure mode, impact force, reaction force, and reinforcements strain were recorded and analysed.

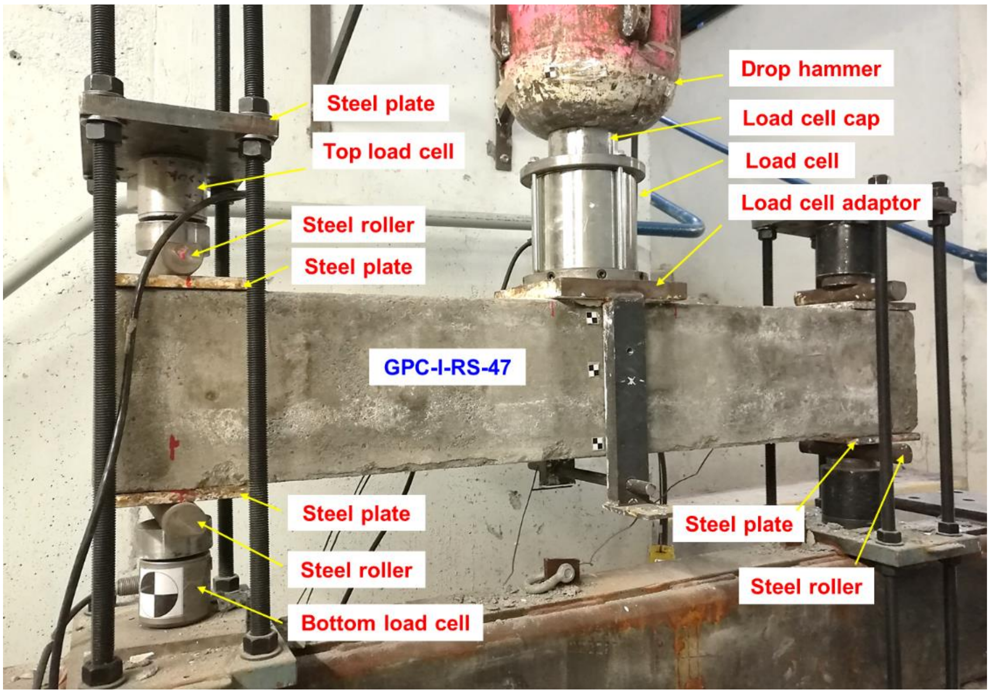

Fig. 4. Impact test setup

3. Quasi-static test results

3.1. Failure modes and crack patterns

Fig. 5 shows the failure modes and crack patterns of the three beams under quasi-static loads. As expected, all the beams failed in diagonal shear since their flexural capacities were much higher than the shear capacities, characterized by a very wide diagonal crack which initiated from the steel v-block and ended at one support. The crack patterns were almost symmetric for the three beams. The similar flexural crack patterns of Beams GPC-S-RS-52 and GPC-S-SP-40 indicated that these two beams had similar flexural performance as expected because they were designed with the same tension reinforcement ratio. The diagonal cracks initiated on Beam GPC-S-NS-34 when the applied load reached about 32 kN as circled in **Fig. 5** (the numbers represent the applied loads), which was less than those (about 46-51 kN) for Beams GPC-S-SP-40 and GPC-S-RS-52 due to the lower compressive strength of concrete and stirrup ratio (0%) of Beam GPC-S-NS-34. Stirrup rupture was observed in both Beams GPC-S-RS-52 and GPC-S-SP-40.

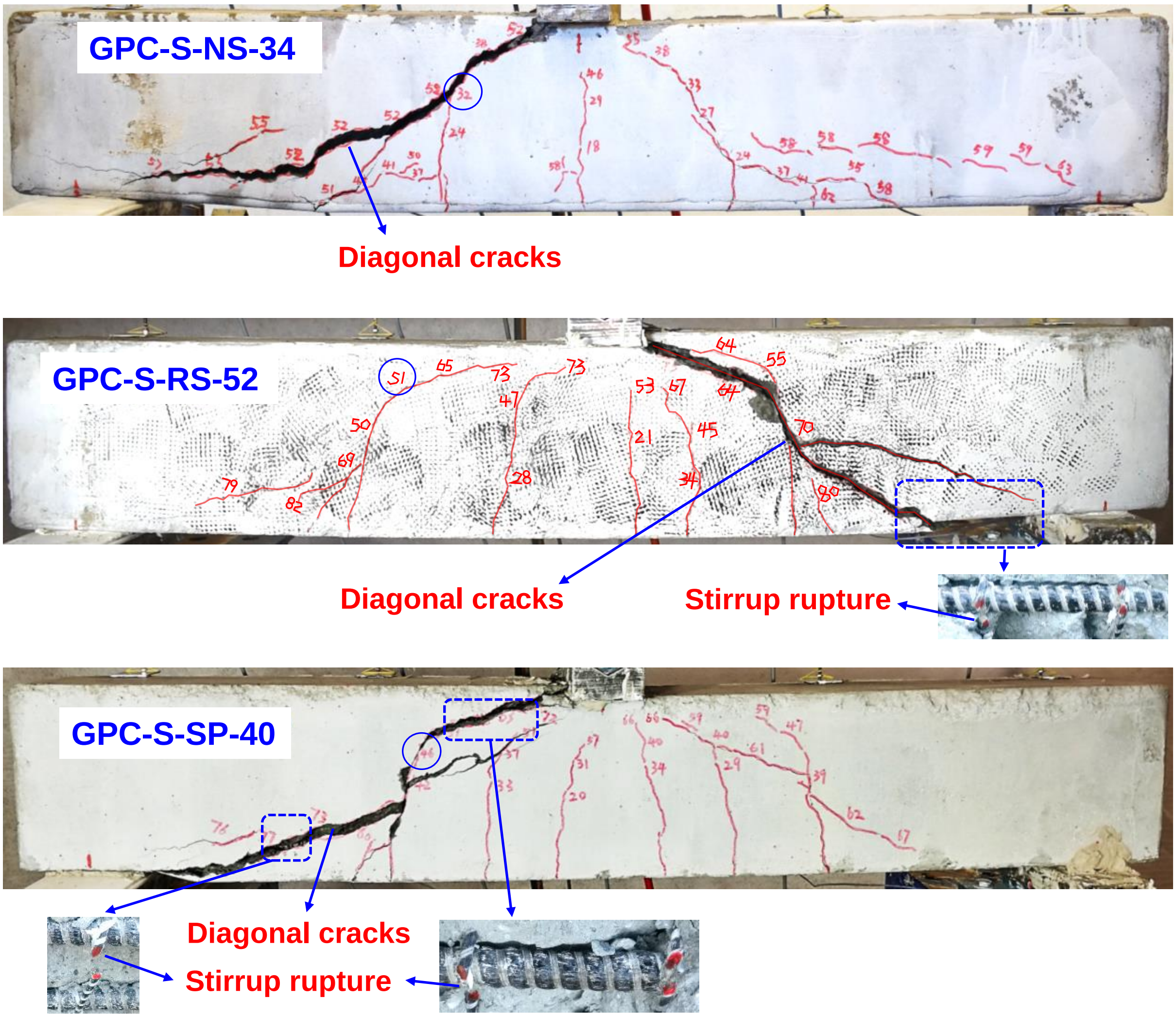

Fig. 5. Failure modes and crack patterns of the three beams under quasi-static loads

3.2. Quasi-static responses

Table 3 gives the quasi-static test results. Since it is believed that the shear resistance contribution from concrete to the beam capacity is proportional to the square root of the compressive strength of concrete [19], the maximum loads (shear capacities) of the three beams were normalized with respect to the square root of the GPC compressive strength $\sqrt{f_c'}bd$ [20, 36-38]. **Fig. 6** shows the normalized load-midspan deflection curves of the three tested beams. It can be seen that all the beams exhibited nearly bilinear load-deflection behaviour up to the maximum loads (i.e., 66.5 kN, 85.2 kN, and 77.3 kN as listed in **Table 3** for Beams GPC-S-NS-34, GPC-S-RS-52, and GPC-S-SP-40, respectively; the corresponding normalized maximum loads were 0.453, 0.469, and 0.485, respectively). In the first linear stage, the three beams had similar uncracked stiffness which were associated with the gross moment of inertia of the beam section while they had varying flexural cracking loads (i.e., 11.0 kN, 21.8 kN, and 20.5 kN as listed in **Table 3** for Beams GPC-S-NS-34, GPC-S-RS-52, and GPC-S-SP-40, respectively) due to different tensile strengths of the GPC material and the reinforcement cage. The existence of stirrups besides provides shear resistance, the reinforcement cage also results in more bending resistance than individual longitudinal bar. A reduced slope with nonlinear segment is identified as the second stage due to the flexural and shear cracks. The normalized maximum loads of Beams GPC-S-RS-52 and GPC-S-SP-40 were 0.469 and 0.485, respectively, while it was 0.453 for Beam GPC-S-NS-34. Therefore, the shear contributions of the conventional rectangular stirrups and the spiral stirrups to the normalized shear capacities of Beams GPC-S-RS-52 and GPC-S-SP-40 were 3.5% and 7.1%, respectively. With the higher normalized shear capacity of GPC-S-SP-40 than that of Beam GPC-S-RS-52, it can be concluded that spiral stirrups could increase the shear capacity of BFRP reinforced GPC beams under static loads as compared to conventional rectangular stirrups. This finding agrees with the results in reference [10] as mentioned above, which could be resulted from the increased dowel action attributed to longitudinal confinement provided by the spiral stirrups [10].

Table 3 Quasi-static test results

Beam	Cracking load (kN)	Maximum load P (kN)	Normalized maximum load $P/bdf_c'^{1/2}$	Midspan deflection at maximum load (mm)	Strain at maximum load (με)			
					Rebar SG1	Rebar SG2	Stirrup SG1	Stirrup SG2
GPC-S-NS-34	11.0	66.5	0.453	9.6	-	4700	*	*
GPC-S-RS-52	21.8	85.2	0.469	8.7	4600	3800	13400	6800
GPC-S-SP-40	20.5	77.3	0.485	7.5	4600	3700	7600	9700

Note: '-': not captured due to strain gauge failure; '*': no stirrup SGs.

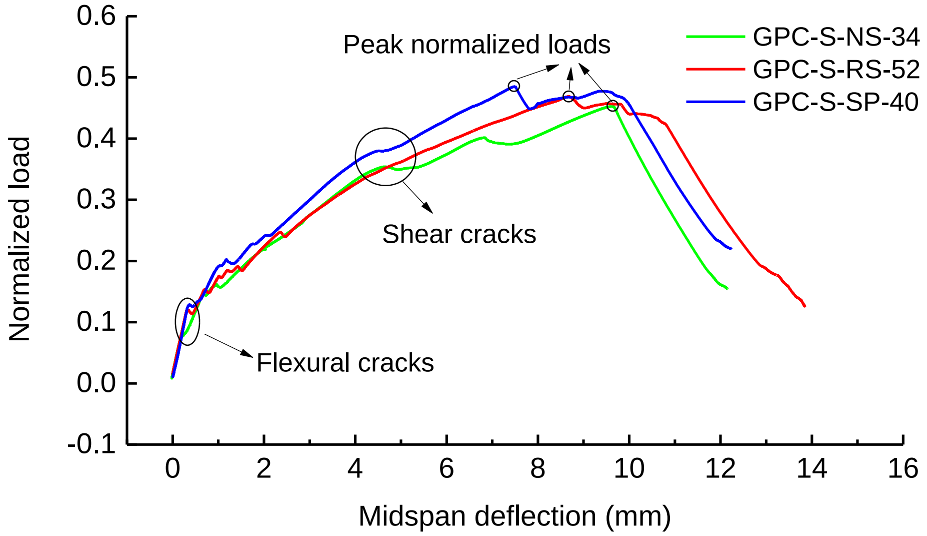

Fig. 6. Normalized load-midspan deflection curves of the three beams

Fig. 7 shows the normalized load-strain curves of the bottom longitudinal reinforcements and the stirrups, which are similar to the normalized load-midspan deflection curves before the failure of the beams. Both the strain of the bottom BFRP bars and the stirrups were very small at uncracked stage prior to flexural cracking since the load carrying was mainly contributed by the GPC material. Once the flexural cracks appeared, the tensile force carried by GPC transferred to tension reinforcements and the strain of the bottom longitudinal reinforcements then increased sharply while the strain of the stirrups increased gradually. With the increased load, the shear cracks appeared and the strain of stirrups increased sharply as expected. The strain of the bottom longitudinal bars (3800-4700 με) at maximum loads was much lower than that of the stirrups (7600-13400 με), indicating the beams failed in a shear-governed manner.

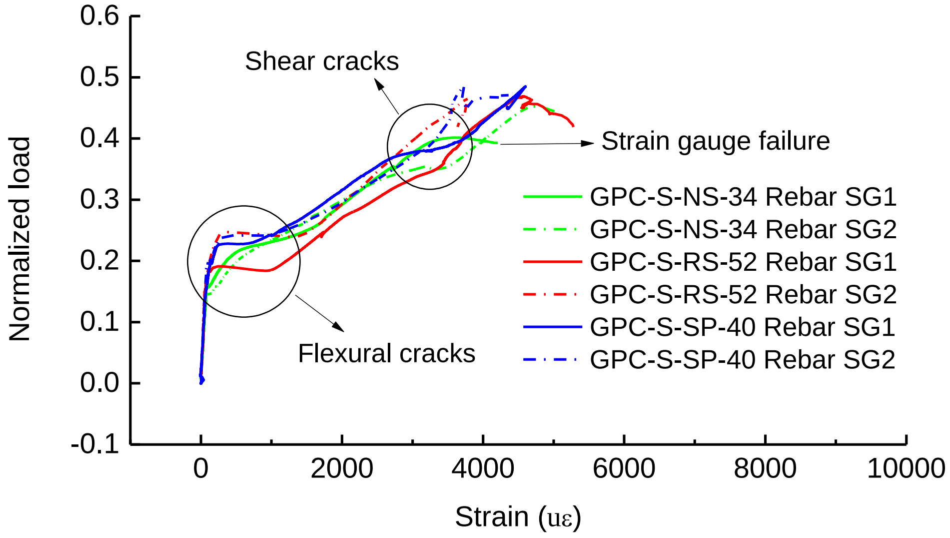

(a)

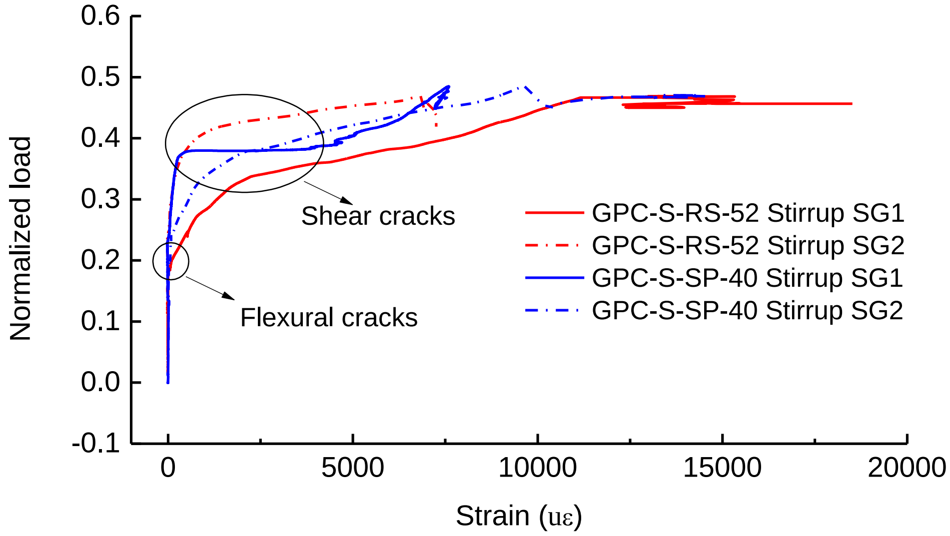

(b)

Fig. 7. Normalized load-strain curves of (a) the bottom reinforcements and (b) the stirrups

Currently, there is no standard available for GPC beams reinforced with FRP bars. Therefore, shear capacities of the GPC beams were predicted based on Standards ACI 440.1R-15 [19] and CSA S806-12 [18], which were for design of OPC beams. **Table 4** gives the ratios of the predicted results to the test results. The CSA S806-12 code gives more accurate predictions with the average ratio of 0.94 while the predictions based on the ACI 440.1R-15 code underestimate the shear capacities of the tested beams with the average ratio of 0.62. This observation is in agreement with the findings by EI Refai and Abed [39], EI-Sayed and Soudki [40], Alam and Hussein [37], Kim and Jang [41], Razaqpur and Spadea [16], and Maranan et al. [10]. The reason could be that the ACI 440.1R-15 code [19] gives more conservative prediction by considering the effect of axial stiffness $\rho_f E_f$ (modulus of elasticity of FRP bars E_f and tension reinforcement ratio ρ_f) of tension FRP bars with a factor k (ratio of depth of neutral axis to reinforcement depth, less than 1.0), as compared to the factor k_r (greater than 1.0) as specified in CSA S806-12 code [18].

Table 4 Ratios of the predicted shear capacities to the test results

Beam	Test shear capacity P (kN)	ACI 440.1R-15 [19]		CSA S806-12 [18]	
		Predicted shear capacity (kN)	Ratio	Predicted shear capacity (kN)	Ratio
GPC-S-NS-34	66.5	44.8	0.68	66.6	1.00
GPC-S-RS-52	85.2	48.2	0.57	77.6	0.91
GPC-S-SP-40	77.3	46.0	0.60	71.2	0.92
Mean			0.62		0.94

4. Impact test results

4.1. Failure modes and crack patterns

As anticipated, both Beams GPC-I-RS-47 and GPC-I-SP-46 failed in shear as shown in **Fig. 8**. Diagonal shear cracks and stirrup rupture were observed. In addition, Beam GPC-I-RS-47 suffered severe splitting damage of the top longitudinal bars. The rebar splitting could occur when FRP bar is subjected to large transverse shear force [42]. Beam GPC-I-RS-47 experienced severer splitting damage of the top longitudinal bars as compared to Beam GPC-I-SP-46, which could be explained as follows: as compared to rectangular stirrups, the longitudinal confinement provided by spiral stirrups could better restrain the widening of cracks, further enhance the dowel action of the bottom longitudinal reinforcements and maintain the shear contribution from aggregate interlocking [10]. Therefore, Beam GPC-I-RS-47 had higher compression and shear stresses in the top longitudinal bars and the compression zone of the beam section than those of Beam GPC-I-SP-46 [21], which led to severer splitting damage to the top longitudinal bars in Beam GPC-I-RS-47 than that in Beam GPC-I-SP-46.

As listed in **Table 5**, Beam GPC-I-RS-47 experienced larger midspan deflection and diagonal shear crack width than Beam GPC-I-SP-46. In addition, as compared to the two Beams GPC-S-RS-52 and GPC-S-SP-40 under static loads, both Beams GPC-I-RS-47 and GPC-I-SP-46 under impact loads experienced severer concrete damage, splitting damage of the top longitudinal bars, but less flexural cracks.

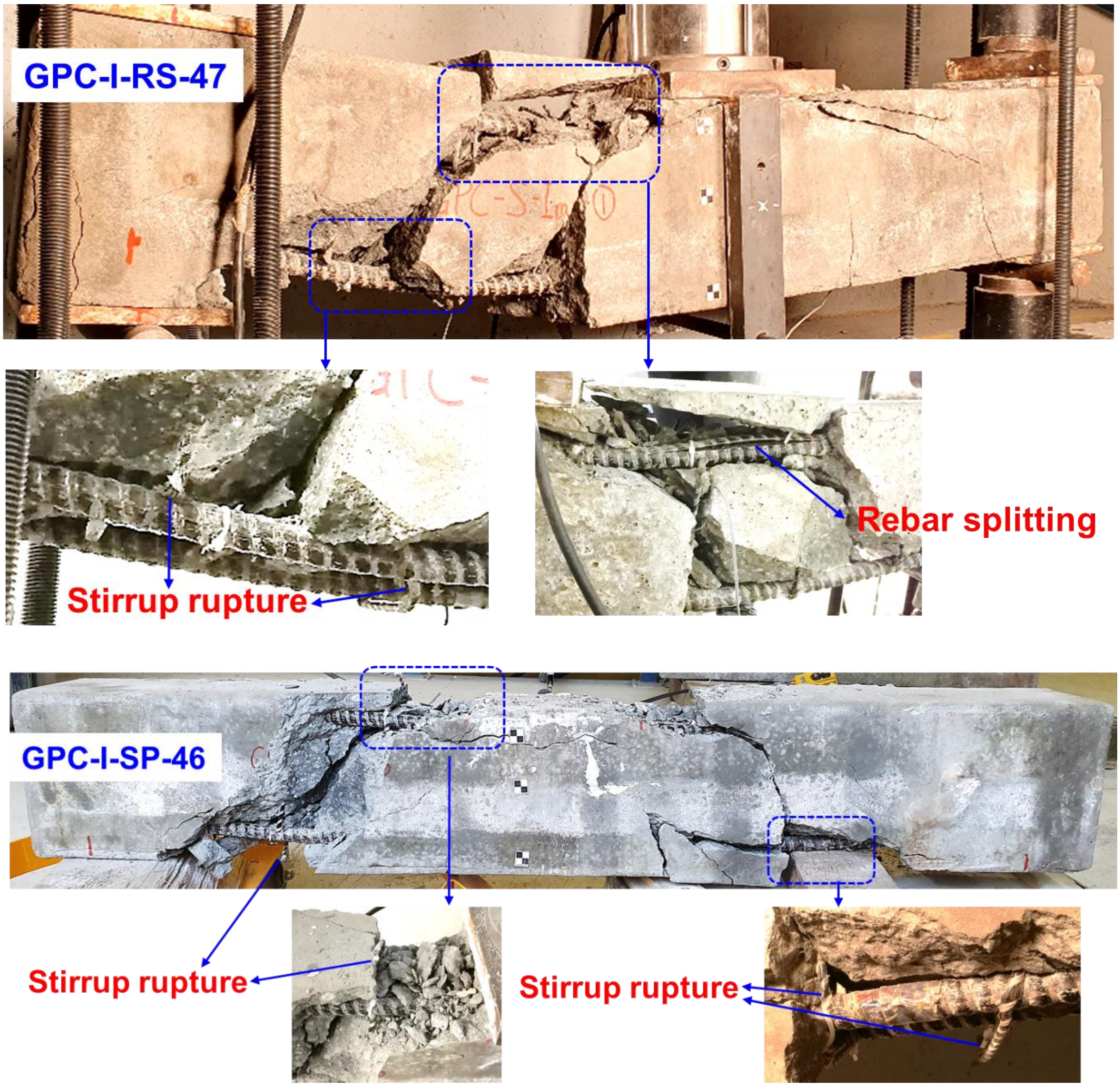

Fig. 8. Failure modes of the two beams under impact loads

The failure progress of the two beams under impact loads are shown in **Fig. 9**. Two vertical flexural cracks at 1 ms and another two shear cracks at 2 ms were observed on both Beams GPC-I-RS-47 and GPC-I-SP-46. As can be seen, the shear crack on the left side of Beam GPC-I-RS-47 extended closer to the load point at 2 ms as compared to that on the right side, the rebar splitting damage thus occurred on the left side of the beam. Beam GPC-I-SP-46 had a more symmetric failure mode as compared to Beam GPC-I-RS-47. In general, no new crack was observed after 6 ms but the existing cracks further widened and extended.

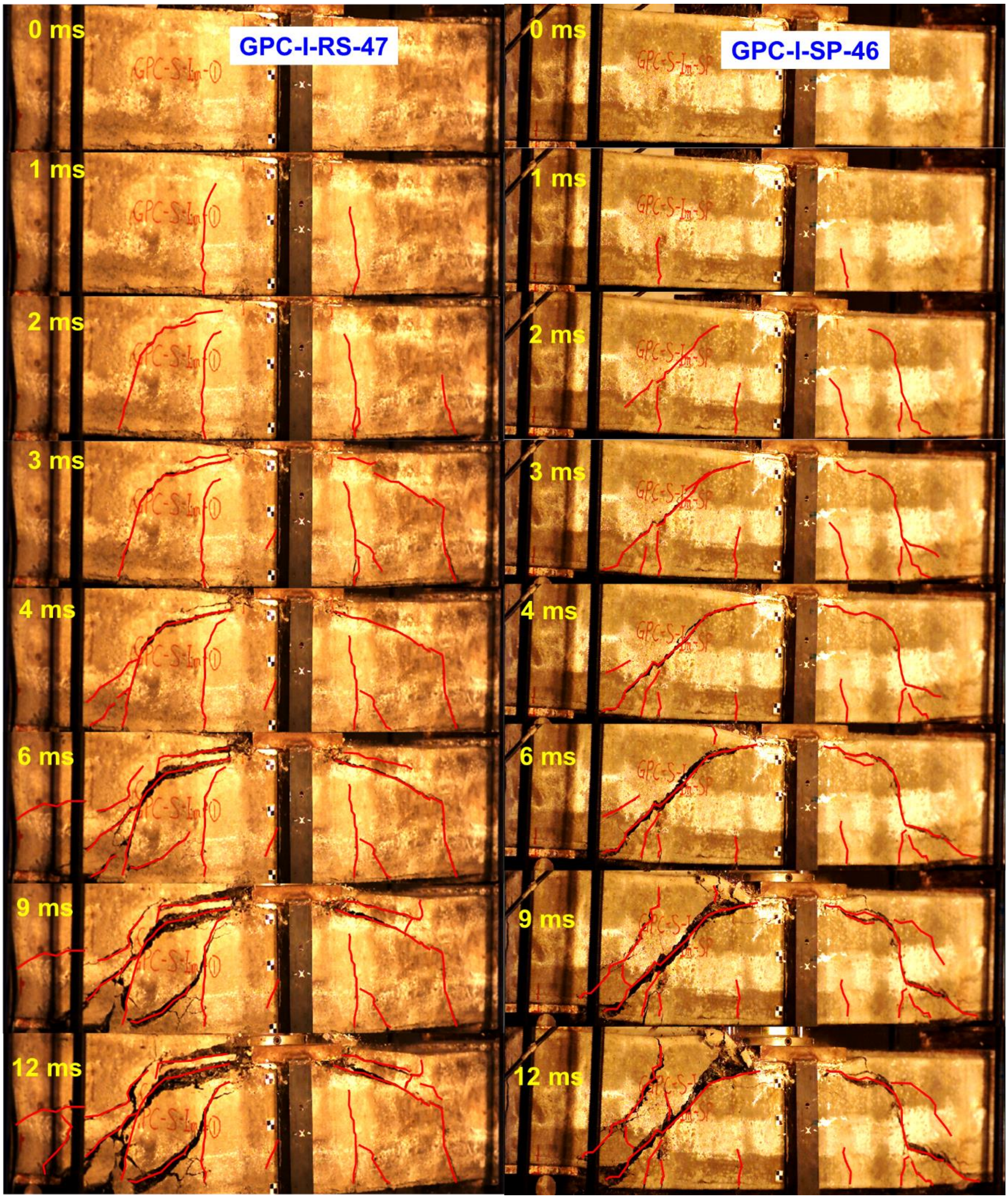

Fig. 9. Failure progress of the two beams under impact loads

4.2. Impact responses

Table 5 gives the impact responses of the tested beams. The time histories of the recorded impact forces and the resultant reaction forces from the bottom load cell and the top load cell are shown in **Fig. 10**. It should be noted that the reaction force of Beam GPC-I-SP-46 was not well recorded and therefore is not shown herein. The two beams showed similar impact force profile, of which the factors have been carefully discussed in [43]. The time histories of the impact forces exhibited a triangular shape with the first peak impact force of about 370-390 kN and the duration about 5 ms. Subsequently, the impact forces reached the second peak of about 125-135 kN and decayed after 10 ms.

Table 5 Impact testing results

Beam	Impact velocity (m/s)	Kinetic energy (J)	Maximum impact force (kN)	Maximum reaction force (kN)	Maximum deflection (mm)	Residual deflection (mm)
GPC-I-RS-47	5.74	3352.4	385.3	115.3	64.0	34.0
GPC-I-SP-46	5.86	3494.1	374.0	-	37.3	13.3

Note: '-': measurement error.

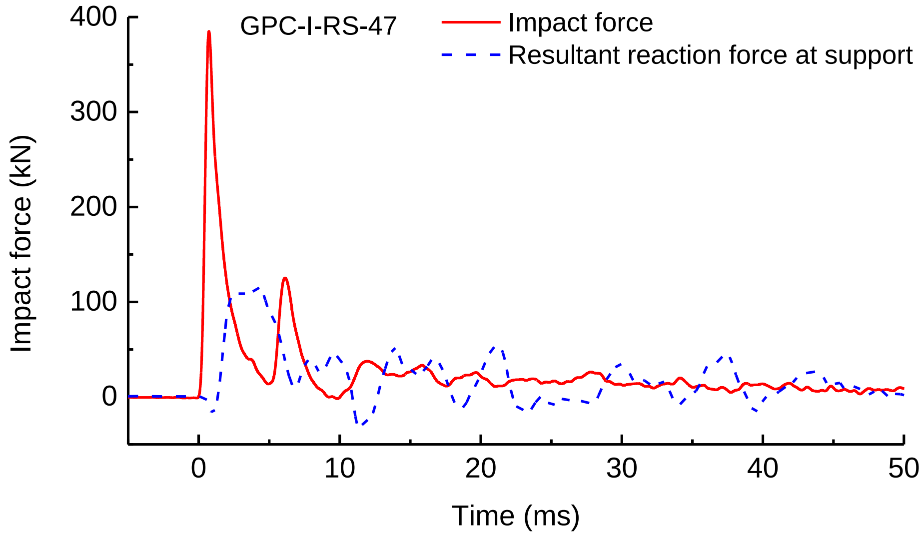

(a)

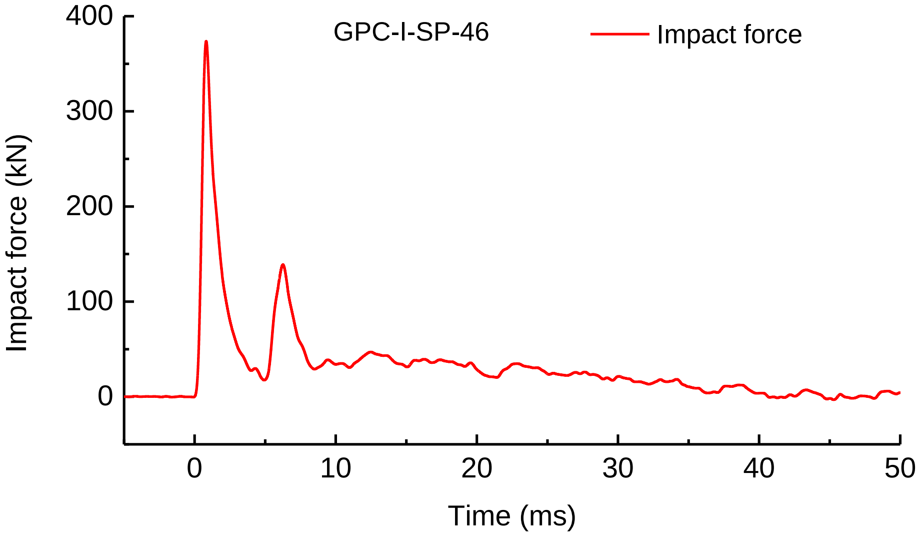

(b)

Fig. 10. Impact and reaction force time histories of Beams (a) GPC-I-RS-47 and (b) GPC-I-SP-46

Fig. 11 displays the midspan deflection time histories of the two beams. The maximum deflection of Beams GPC-I-RS-47 and GPC-I-SP-46 was 64.0 mm and 37.3 mm, respectively, while their residual deflection was 34.0 mm and 13.3 mm, respectively. The maximum and residual deflection of Beam GPC-I-RS-47 at midspan was much larger than that of Beam GPC-I-SP-46 due to the severer splitting damage of the top longitudinal bars of GPC-I-RS-47. Therefore, it can be concluded that the stirrup type has a significant effect on the shear behaviour of GPC beams reinforced with BFRP bars under impact loads and the spiral stirrups demonstrated superior impact performance than the rectangular stirrups.

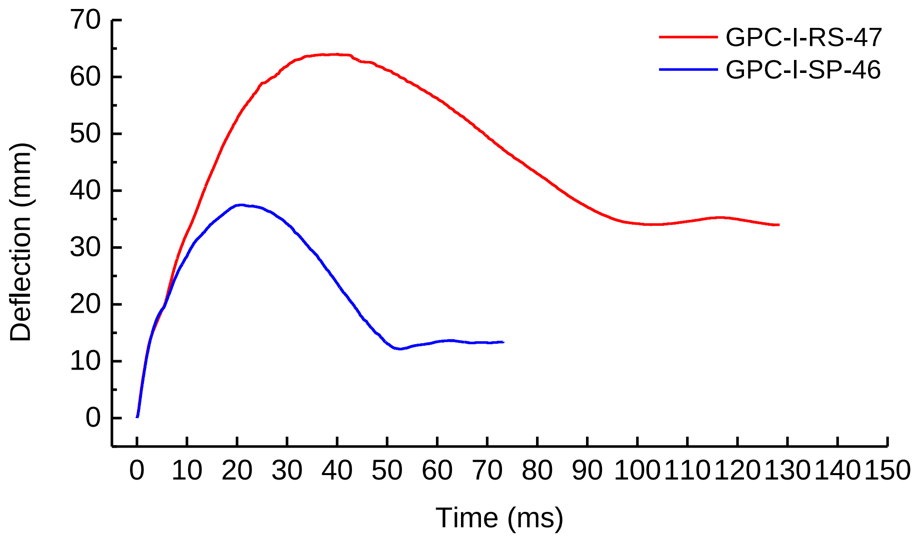

Fig. 11. Midspan deflection time histories of the two beams

Fig. 12 shows the reinforcement strain time histories of the two beams. Both Beams GPC-I-RS-47 and GPC-I-SP-46 experienced the peak strain of the bottom longitudinal bars (rebar SG1 and rebar SG2) about 6000 με. The stirrup SG2 in Beam GPC-I-RS-47 had larger peak than that of SG1 due to the severer shear damage on the left side of the beam. It should be noted that some strain gauges (rebar SG2 and stirrup SG2 in Beam GPC-I-RS-47, rebar SG2 and rebar SG1 in Beam GPC-I-SP-46) were not recorded in full due to the rupture of strain gauge cables. The stirrup SG2 and stirrup SG1 in Beam GPC-I-SP-46 failed immediately after the impact and their data therefore are not presented herein.

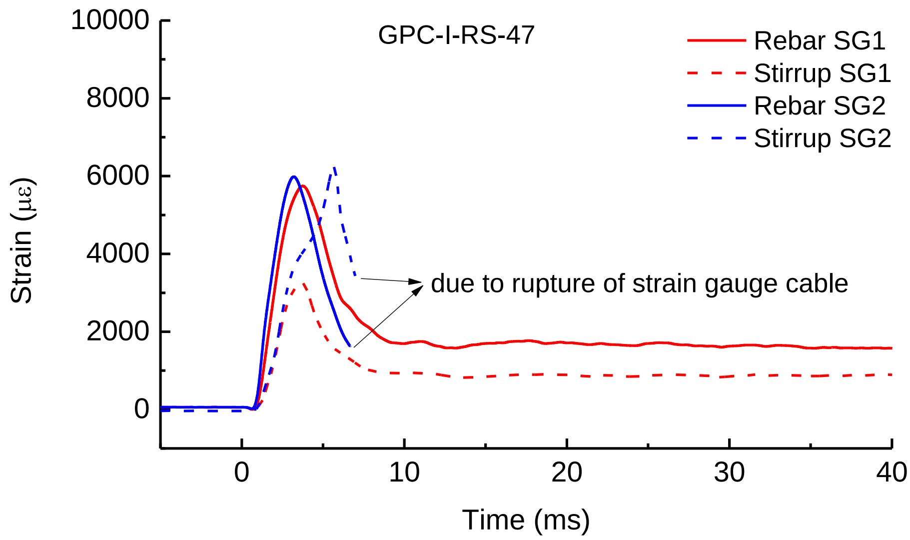

(a)

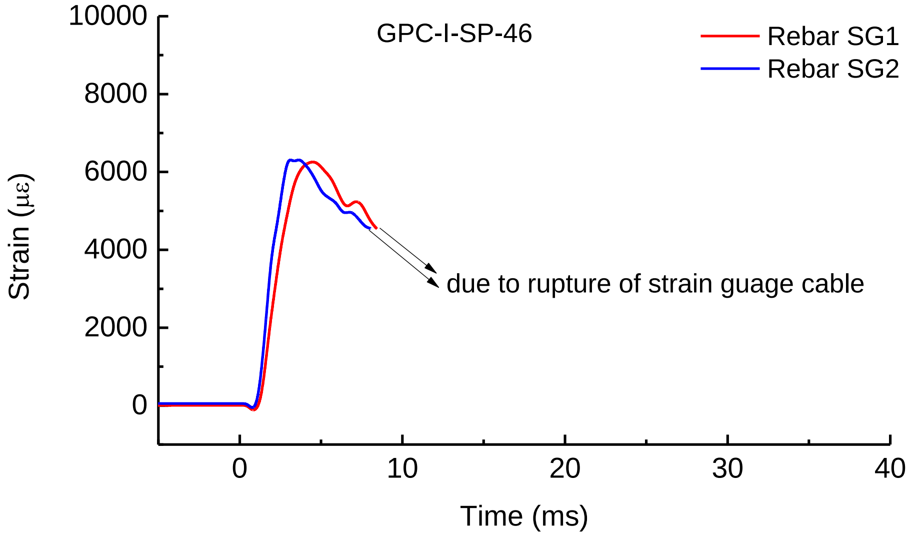

(b)

Fig. 12. Strain time histories of reinforcements: (a) GPC-I-RS-47 and (b) GPC-I-SP-46

5. Numerical simulation

5.1. Finite element model

Numerical models of the tested beams were developed by using LS-DYNA [44]. Following the test set-up, parts of GPC beams, reinforcements, steel plates, steel rollers, drop hammer, load cell, load cell cap, as well as the load cell adaptor were included in the model as shown in **Fig. 13**. Eight-node solid elements were employed for all the parts except the reinforcements. Hughes-Liu beam elements with cross section integration were adopted for the reinforcements. The keyword *Constrained_Beam_in_Solid was used to model the interaction between the reinforcements and the concrete. *Automatic_Surface_to_Surface contact was utilized for simulating the contacts among all the parts, except that *Automatic_Surface_to_Surface_Tiebreak contact was employed to model the connection between the load cell adaptor and the load cell. The keyword *Initial_Velocity_Generation was used to specify the initial impact velocity of 5.8 m/s for the drop hammer according to the test results. Mesh size sensitivity analysis was conducted. The mesh size of 5 mm was determined for GPC beam and reinforcements and the mesh size of 10 mm was adopted for the other parts by balancing the computational accuracy and cost.

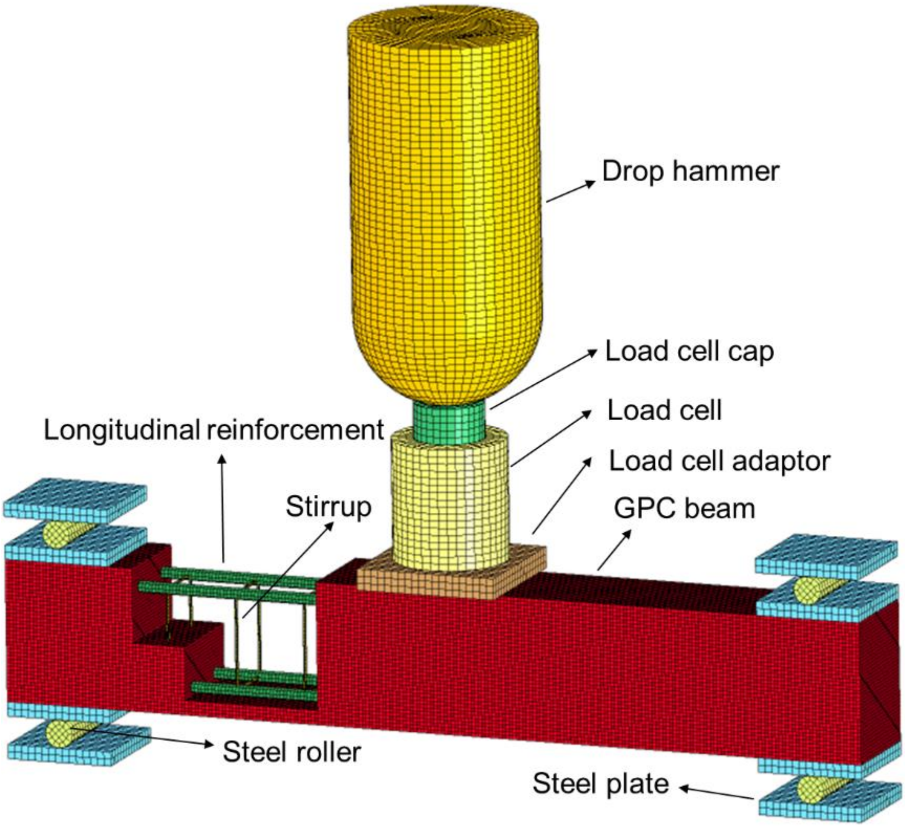

Fig. 13 Numerical model of Beam GPC-I-RS-47

5.2. Material models

There are several material models available in LS-DYNA [45] to simulate the behaviour of OPC material, such as *Mat_Pseudo_Tensor (*Mat_016), *Mat_Concrete_Damage_Rel3 (*Mat_072R3, also called KCC model), *Mat_Johnson_Holmquist_Concrete (*Mat_111), *Mat_CSCM_Concrete (*Mat_159), *Mat_Concrete_Damage_Plastic_Model (*Mat_273), etc. However, these models cannot be directly applied to GPC, ultra-high performance concrete (UHPC), and ultra-high performance fiber reinforced concrete (UHPFRC) due to the different material properties, e.g., GPC is more brittle than OPC and behaves differently in softening stage [27, 28, 46]. There is no verified material model for GPC yet. It is worth noting that KCC model has been used to simulate UHPC [47] and UHPFRC structures [48] under impact and blast loads after modification and calibration of the material model. Since KCC model could take the effects of strain hardening, damage, strain softening, as well as strain rate effect into consideration [49], it has been widely used for the simulations of concrete structures subjected to impact and blast loads [50-53]. In this study, the KCC model was also used and modified to simulate GPC material. Before modification, three GPC cylinders with the average strength of 40 MPa were tested as per AS 1012.9:2014 [54] to obtain the stress-strain curve. The testing data are used to calibrate the modified KCC model in representing the GPC material properties as shown in **Fig. 14**.

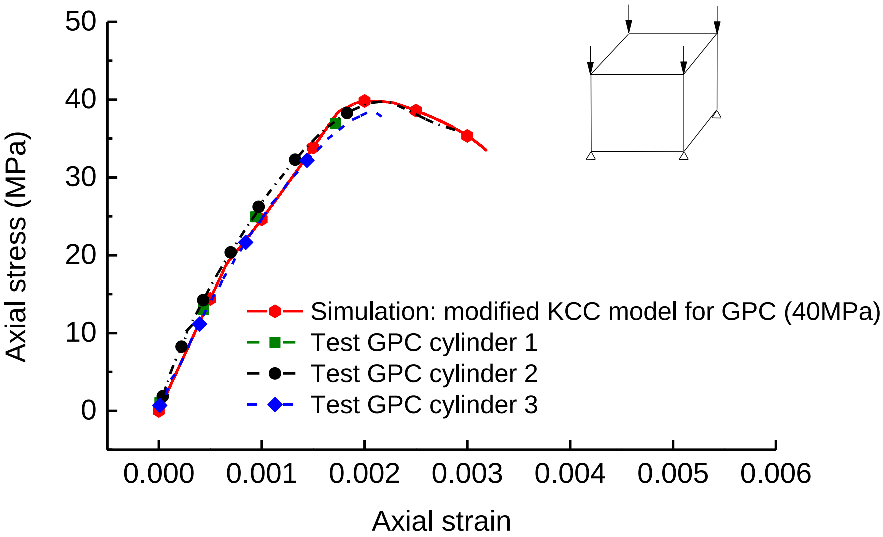

Fig. 14 Comparison of stress-strain curves of the test and numerical results

KCC model defines three failure surfaces (i.e. yield surface $\Delta\sigma_y$, maximum failure surface $\Delta\sigma_m$, and residual failure surface $\Delta\sigma_r$) with eight parameters (i.e. a_{0y}, a_{1y}, a_{2y}, a_{0m}, a_{1m}, a_{2m}, a_{1r} and a_{2r}) as follows [49]:

$$\Delta\sigma_y = a_{0y} + \frac{p}{a_{1y}+a_{2y}p} \tag{1}$$

$$\Delta\sigma_m = a_{0m} + \frac{p}{a_{1m}+a_{2m}p} \tag{2}$$

$$\Delta\sigma_r = \frac{p}{a_{1r}+a_{2r}p} \tag{3}$$

where $p = -(\Delta\sigma_{xx}+\Delta\sigma_{yy}+\Delta\sigma_{zz})/3$ is the pressure. **Table 6** lists the modified parameters of the GPC material with compressive strength of 40 MPa (see GPC-1), which are used for material calibration in simulation against the test data of cylinders as shown in **Fig. 14**. The modification was defined as follows: due to the lack of test data, a similar tensile strength (i.e., 3.8 MPa) for the GPC material to the default value (i.e. 3.5 MPa) for OPC was adopted (see **Table 6**) to get good consistence between the beam simulation and the test results in Section 5.3. In KCC model, the yield strength $\Delta\sigma_y$ of OPC is taken as 0.45 times of the maximum strength $\Delta\sigma_m$. Based on the stress-strain curves of GPC cylinders in **Fig. 14**, the yield strength of GPC is estimated as 19.0 MPa, which is about 0.5 times of the maximum strength. Therefore, a_{0y} could be calculated according to Eq.(1) by keeping a_{1y}, a_{2y} unchanged as defined in the KCC model. Since OPC and GPC with the same compressive strength of 40 MPa have the same maximum strengths, the parameters of GPC in maximum failure surface (a_{0m}, a_{1m}, and a_{2m}) are not changed. Both a_{1r} and b_1 (parameter related to the compressive damage behaviour of concrete) have very significant effect on the concrete behaviour at post-failure stage, which need be modified, while a_{2r} was kept unchanged as listed in **Table 6** (see GPC-1). The damage function $\eta(\lambda)$ is a user-defined function of effective plastic strain λ as shown in **Fig. 15**, which was based on the stress-strain relation of the GPC material test data.

Table 6 Key parameters used in KCC model for GPC

Material	OPC (default)	GPC-1	GPC-2
Compressive strength (MPa)	40	40 (for GPC material calibration)	47 (for beam simulation)
Tensile strength (MPa)	3.5	3.8	4.0
Density (kg/m^3)	2300	2300	2300
Poisson's ratio	0.19	0.19	0.19
a_{0y}	8.928E6	9.489E6	1.115E7
a_{1y}	0.625	0.625	0.625
a_{2y}	6.437E-9	6.435E-9	5.477E-9
a_{0m}	1.182E7	1.183E7	1.390E7
a_{1m}	0.4463	0.4463	0.4463
a_{2m}	2.020E-9	2.020E-9	1.719E-9
a_{1r}	0.4417	0.3334	0.3334
a_{2r}	2.958E-9	2.958E-9	2.517E-9
b_1	1.6	0.6	0.6

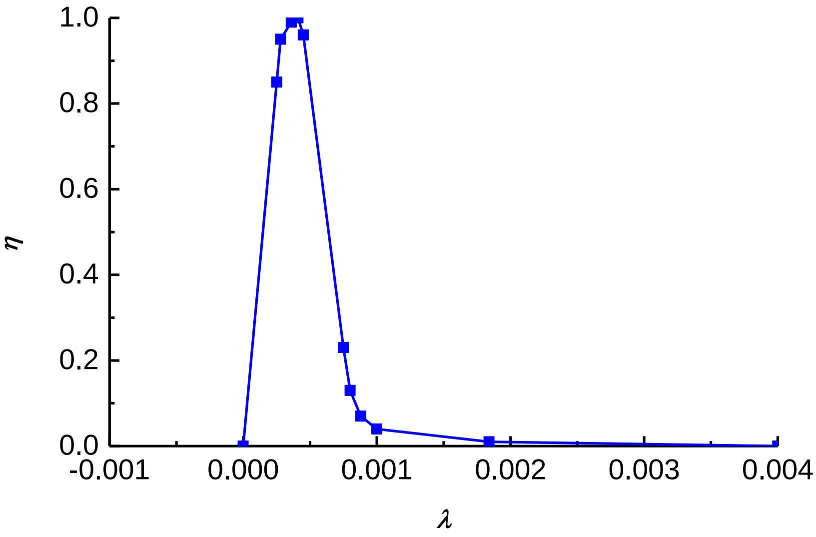

Fig. 15 Damage function $\eta(\lambda)$ for GPC

With the above modified parameters, GPC compression test with single element [48, 55] in LS-DYNA was conducted to obtain the stress-strain curve and compared to the cylinder test results as shown in **Fig. 14**. As can be seen, KCC model with the modified parameters is able to capture the behaviour of GPC material under compression test.

Although the parameters of GPC material with compression strength of 40 MPa were calibrated, the GPC material parameters of Beams GPC-I-RS-47 and GPC-I-SP-46 are yet confirmed due to different compressive strengths. In KCC model, scaling of failure surfaces is usually used to solve this problem. To model a new GPC with known axial compressive strength $f'_{c,new}$ (e.g., 47 MPa), its failure surfaces could be scaled from a known GPC material with the axial compressive strength $f'_{c,old}$, e.g., GPC-1 with the compressive strength of 40 MPa in this study, as follows [49]:

$$\Delta\sigma_{new} = a_{0,new} + \frac{p}{a_{1,new}+a_{2,new}p} \tag{4}$$

where the new coefficients ($a_{0,new}$, $a_{1,new}$, $a_{2,new}$) of failure surfaces are expressed in terms of the old ones as $a_{0,new} = ra_{0,old}$, $a_{1,new} = a_{1,old}$, $a_{2,new} = a_{2,old}/r$, in which r is the scaling factor defined by the ratio of compressive strengths, i.e., $f'_{c,new}/f'_{c,old}$. Therefore, the eight parameters of three failure surfaces in KCC model for Beam GPC-I-RS-47 with GPC compressive strength of 47 MPa could be obtained and listed in **Table 6** (see GPC-2), corresponding to a factor *r* of 1.175 (i.e., 47 MPa/40 MPa). Because the tensile strength of concrete is proportional to the square root of compressive strength [56], the tensile strength was scaled to 4.0 MPa by the square root of the scaling factor (i.e., 1.175). The other parameters in KCC model remained unchanged as those with the compressive strength of 40 MPa (GPC-1). Because of the very little difference between the GPC compressive strengths of Beams GPC-I-RS-47 and GPC-I-SP-46, the parameters for GPC with compressive strength of 47 MPa were also utilized for Beam GPC-I-SP-46.

*Mat_Piecewise_Linear_Plasticity (*Mat_024) was employed to model steel and BFRP materials. Load cell was simplified as a solid cylinder. To consider the configuration of internal gap inside the load cell, the equivalent mass density of the load cell was simply determined by the ratio of the actual mass to the external volume of the modelled load cell, which was 5850 kg/m^3, about 25% lower than the actual mass density of steel material. For simplicity and without changing the propagating velocity of stress wave inside the load cell, the equivalent modulus of the modelled load cell was also taken as 25% lower than the actual modulus of steel material, which was 150 GPa. The values of the parameters used in the beam simulation are listed in **Table 7**.

Table 7 Parameters of material model

Part	Material model in LS-DYNA	Parameter	Value
GPC beam	*Mat_Concrete_Damage_Rel3 (*Mat_072R3)	See **Table 6** (GPC-2)	See **Table 6** (GPC-2)
BFRP reinforcements	*Piecewise_Linear_Plasticity (*Mat_024)	Density	2000 kg/m^3
		Modulus of elasticity	55 GPa
		Poisson's ratio	0.25
		Strength	1200 MPa
		Failure strain	1.0E-5
Load cell	*Piecewise_Linear_Plasticity (*Mat_024)	Density	5850 kg/m^3
		Modulus of elasticity	150 GPa

		Poisson's ratio	0.3
		Yield stress	500 MPa
Steel plates, steel rollers, drop hammer, load cell cap, load cell adaptor	*Piecewise_Linear_ Plasticity (*Mat_024)	Density	7800 kg/m^3
		Modulus of elasticity	200 GPa
		Poisson's ratio	0.3
		Yield stress	500 MPa

The strength increment due to strain rate effect of BFRP composites [57] and steel material [58] was considered in material model *Mat_024 by defining the dynamic increase factor (DIF) at given strain rates. The DIF of GPC material was based on dynamic material testing data and the references [59, 60]. In order to model the failure mode of the beams, the erosion algorithm was used by defining erosion criteria through the keyword *Mat_Add_Erosion, which has been widely utilized in concrete structures subjected to impact and blast loads [51-53, 61]. In the present study, erosion criteria were determined by trial-and-error to reach good agreement with the test results as follows: minimum principal strain of -0.12 ('-' denotes tension) and maximum principal strain of 1.8 for concrete, shear strain of 0.009 for the top longitudinal bars, and failure strain of 1.0E-5 [62] as listed in **Table 7** for the bottom longitudinal bars were adopted for both Beams GPC-I-RS-47 and GPC-I-SP-46. Minimum principal strain of -0.012 ('-' denotes tension) and -0.007 was determined for rectangular stirrups and spiral stirrups, respectively.

5.3. Comparison between numerical and test results

The concrete damage level could be characterized by element erosion and effective plastic strain in KCC model. **Fig. 16** compares failure progress of Beam GPC-I-RS-47 between the numerical and test results. As can be seen, the concrete damage predicted by numerical simulation is in good agreement with the crack patterns in the test results. High effective plastic strain appeared on both sides of the beam in the simulation. Severe element erosion initiated from the load cell adaptor was observed on the left side of the beam in the simulation, replicating the wide diagonal shear crack and concrete spalling in the test results. In addition, a number of elements of the top longitudinal bars were deleted in the simulation, indicating the splitting damage of the top BFRP bars in the test. It should be noted that the effective plastic strain contours are not symmetric, which could be due to the numerical errors induced by explicit solver of nonlinear problems and numerical instability caused by softening post-failure characteristics of material models [63]. When material enters softening phase, the symmetry of the numerical results is very sensitive to the numerical errors and the micro-cracks could cause asymmetry [64, 65]. Therefore, the effective plastic strain contour in the simulation at 1 ms is not perfectly symmetric, but symmetric in general as shown in **Fig. 16**. This asymmetry could be also found in references [61, 64, 66, 67]. As time progresses, the level of asymmetry is enhanced, e.g. at 15 ms and 105 ms. It is due to the accumulated asymmetry of numerical results. In addition, the element erosion of reinforcements and concrete for shear-failure-type beams could further aggravate the asymmetry of numerical results, as also found in references [68, 69].

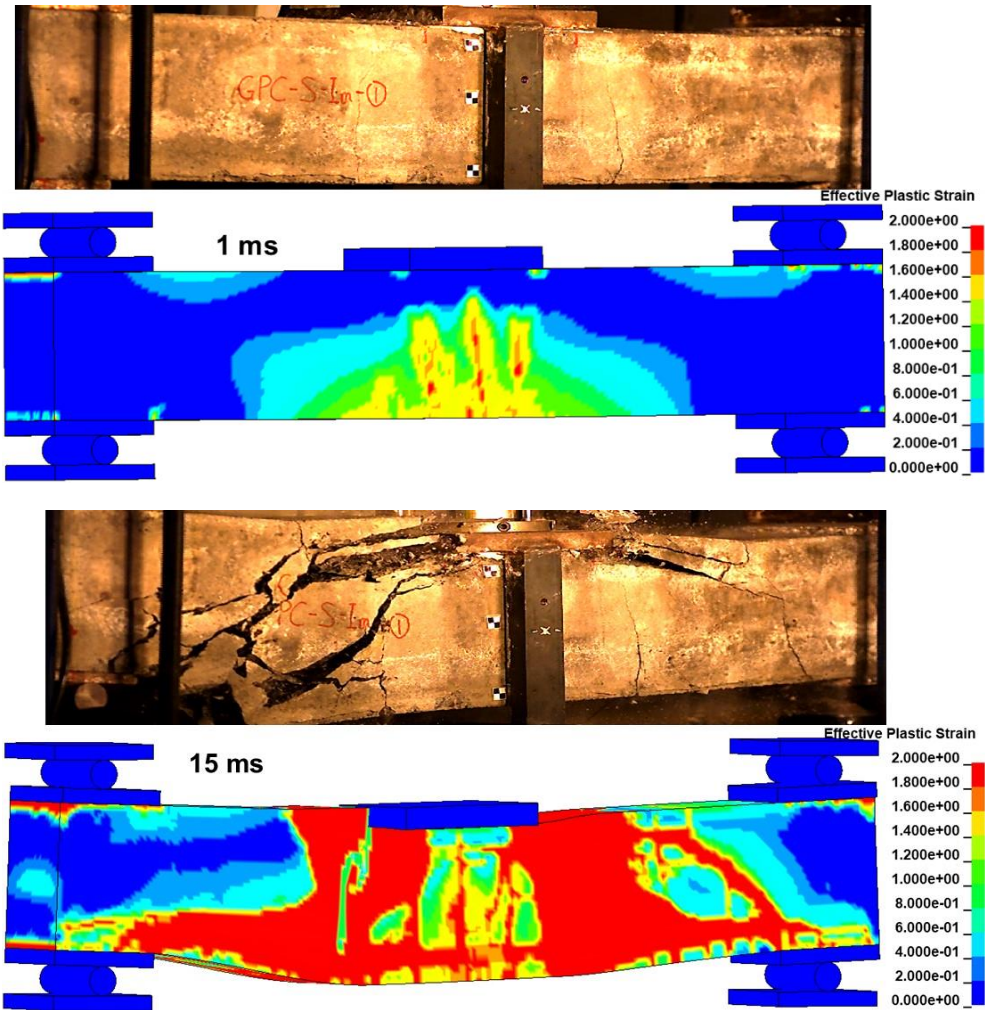

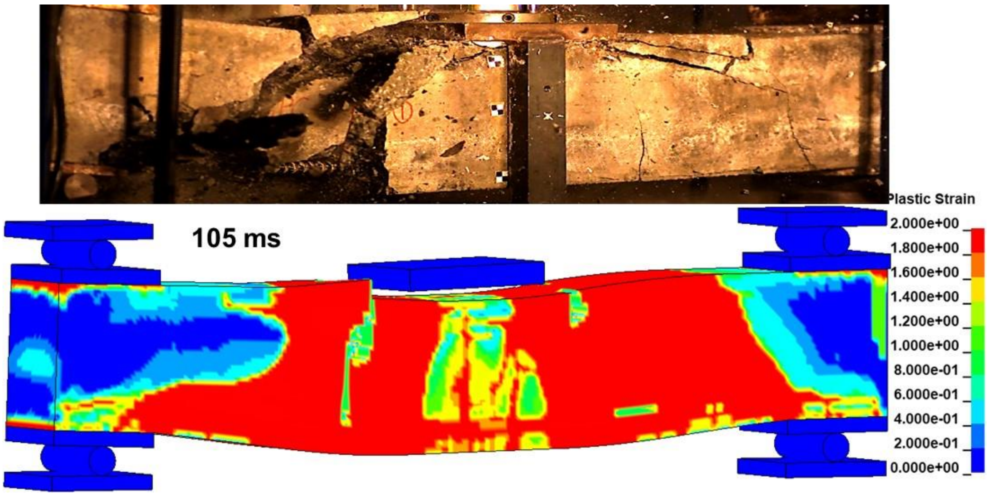

Fig. 16 Comparison of crack pattern and failure progress of Beam GPC-I-RS-47

Fig. 17 shows the comparison of the impact responses of Beam GPC-I-RS-47 between the numerical and test results. The predicted impact force was obtained by the vertical contact force between the load cell and the load cell cap. The peak impact forces from the numerical and test results were 357.9 kN and 385.3 kN, respectively. The maximum deflection from the numerical and test results was 55.5 mm and 64.0 mm, respectively. The corresponding residual deflection was 33.6 mm and 34.0 mm, respectively. The numerical results agree well with the testing results.

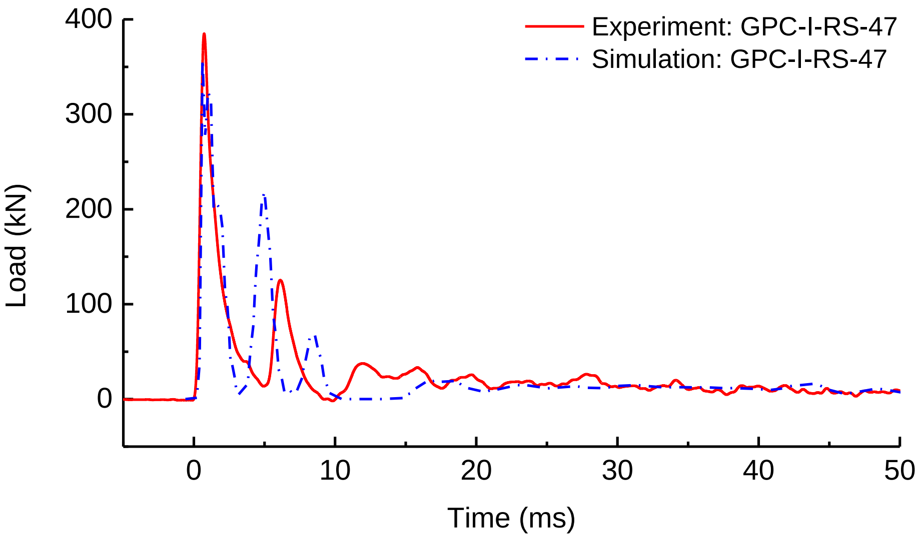

(a)

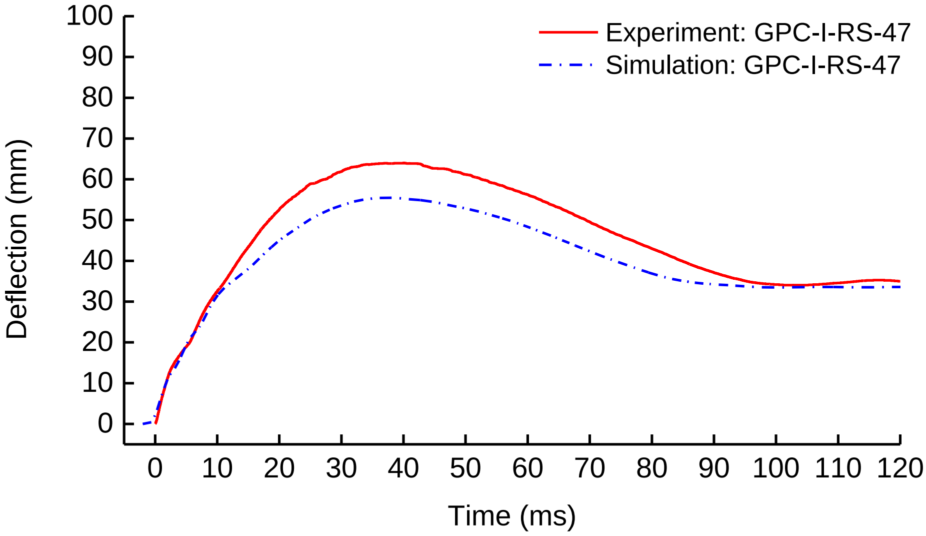

(b)

Fig. 17 Comparison of dynamic responses of Beam GPC-I-RS-47: (a) impact force and (b) midspan deflection

Fig. 18 displays the failure progress of the tested Beam GPC-I-SP-46 and the corresponding effective plastic strain contours in the numerical simulation. It shows that the concrete damage predicted by the numerical simulation resamples the crack patterns in the test results. High effective plastic strain initiated from the load cell adaptor appeared on both sides of the beam. As compared to the simulation of Beam GPC-I-RS-47, less elements of the top longitudinal bars were deleted, indicating that Beam GPC-I-SP-46 experienced less splitting damage of the top longitudinal bars.

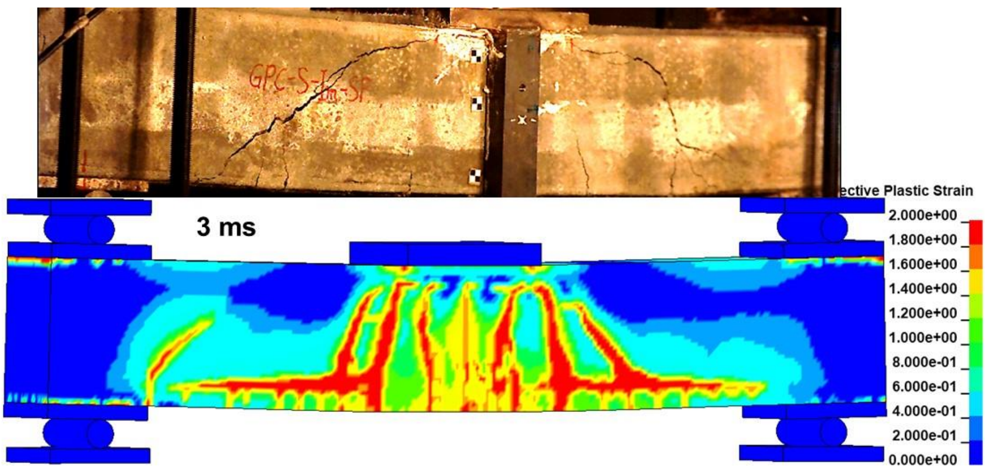

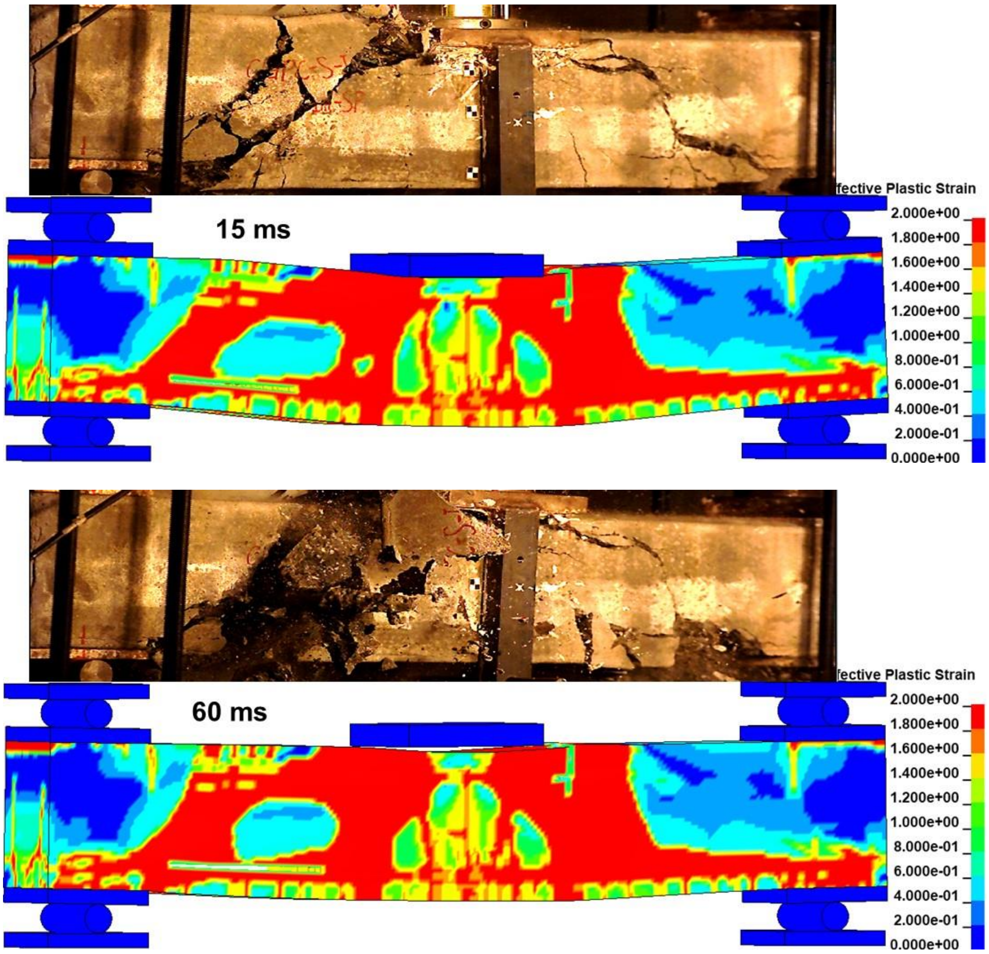

Fig. 18 Comparison of crack pattern and damage progress of Beam GPC-I-SP-46

Fig. 19 shows the comparison of the impact responses of Beam GPC-I-SP-46 between the numerical and test results in terms of impact load profile and midspan deflection. The peak impact forces from the numerical and test results were 357.9 kN and 374.0 kN, respectively. The maximum deflection from the numerical and test results was 32.4 mm and 37.3 mm, respectively. The corresponding residual deflection was 15.8 mm and 13.3 mm, respectively. The predicted impact responses agree well with the test results.

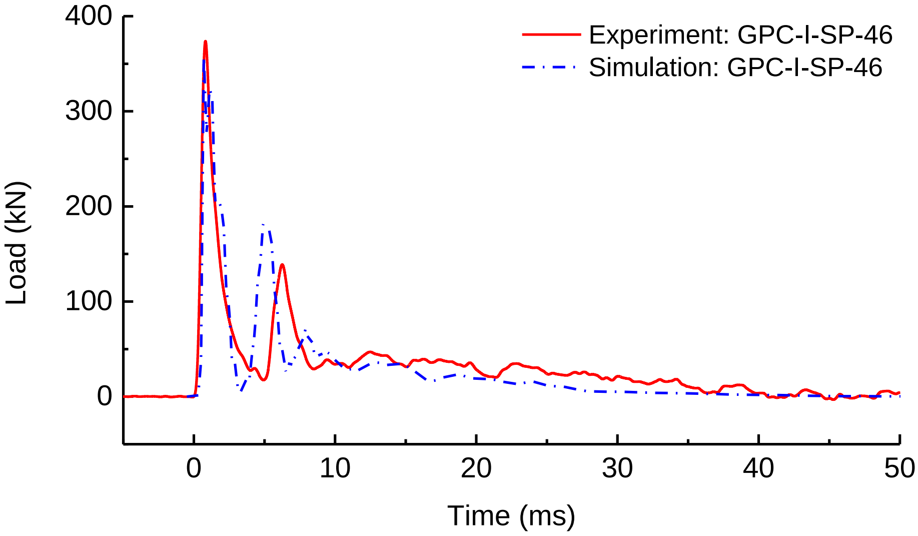

(a)

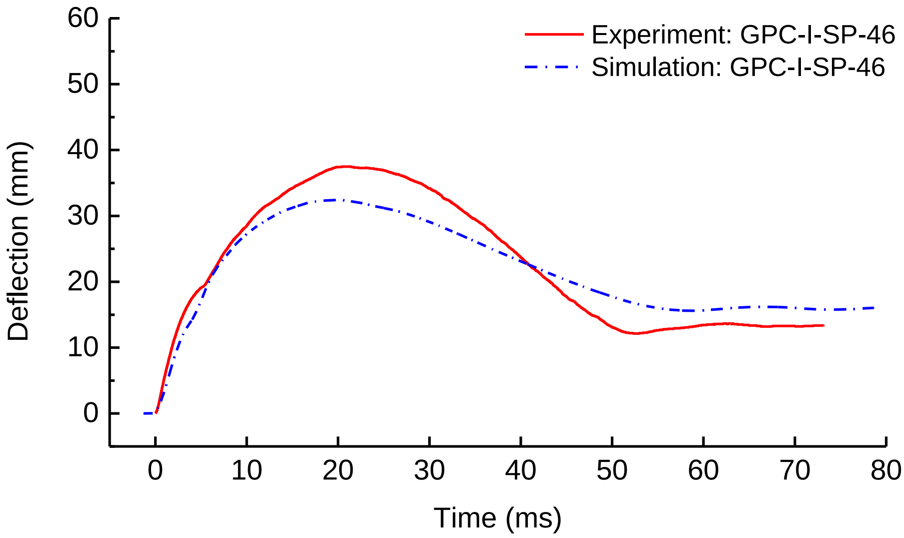

(b)

Fig. 19 Comparison of dynamic responses of Beam GPC-I-SP-46: (a) impact force and (b) midspan deflection

6. Parametric study

With the calibrated numerical models, parametric studies were conducted on Beam GPC-I-RS-47 with commonly used conventional rectangular stirrups. According to design guideline of Standards CSA S806-12 [18] and ACI 440.1R-15 [19], shear strength is mainly contributed by two parts: one is the shear resistance provided by concrete, which is influenced by concrete compressive strength and tension reinforcement ratio (contributed by dowel action and aggregate interlocking); the other is the shear resistance provided by FRP stirrups, which is affected by stirrup ratio. Therefore, the parameters including compressive strength of GPC material, tension reinforcement ratio, and stirrup ratio were considered here. Moreover, in order to avoid splitting damage of compression FRP reinforcements which could further induce severe damage of concrete beams as observed in the tests, the effect of compression reinforcement type was also investigated in the parametric study.

6.1. Effect of GPC compressive strength

Compressive strengths of 27 MPa, 47 MPa, and 67 MPa were specified for three Beams B-27, B-47, and B-67, respectively to study the influences of concrete strength on the beam responses, while all the other parameters were kept the same as the above. The erosion criteria for different compressive strength were assumed as the same in the present study. **Fig. 20** shows the effective plastic strain contours and midspan deflection time histories of the beams with different GPC compressive strength. As can be seen, decreasing GPC compressive strength from 47 MPa to 27 MPa resulted in larger midspan deflection and severer damage to the beam under impact loads. Increasing GPC compressive strength from 47 MPa to 67 MPa only slightly reduced the maximum midspan deflection of the beam by 5% (from 55.5 mm to 52.8 mm) but the residual deflection increased by 27% instead (from 33.6 mm to 42.6 mm). As compared to Beam B-47, Beam B-67 experienced severer splitting damage of the top BFRP bars and more concrete damage and concrete spalling as circled in **Fig. 20** (a). The possible reasons are given as follows: for high strength concrete, more energy is absorbed by every single crack because the total number of cracks are less due to higher tensile strength and fracture energy of concrete [70] as compared to normal strength concrete, leading to less number but wider cracks on beams with high strength concrete than those with normal strength concrete. Thus, after the first peak, Beam B-67 suffered more shear resistance loss due to the weakened dowel action with wider cracks, as compared to Beam B-47. As a result, Beam B-67 was prone to experience more concrete damage and severer splitting damage of top BFRP bars as shown in **Fig. 21** when it was subjected to the second impact (at 5-8 ms) as compared to Beam B-47.

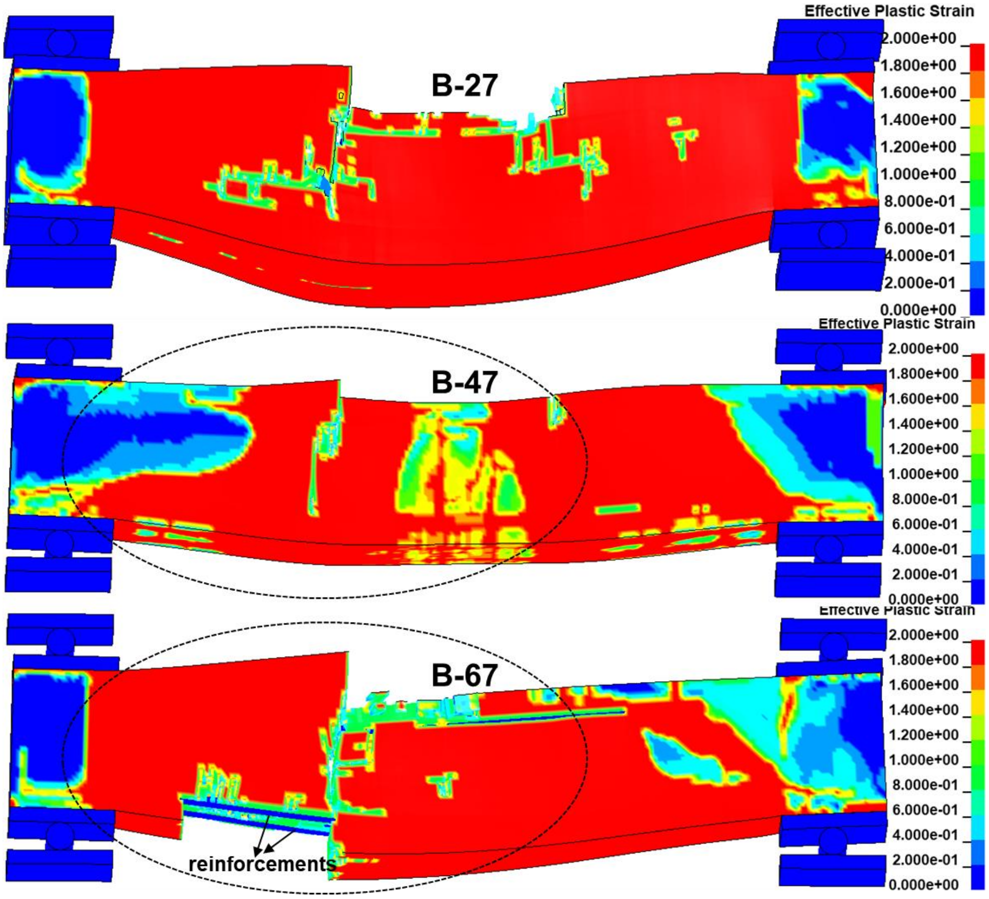

(a)

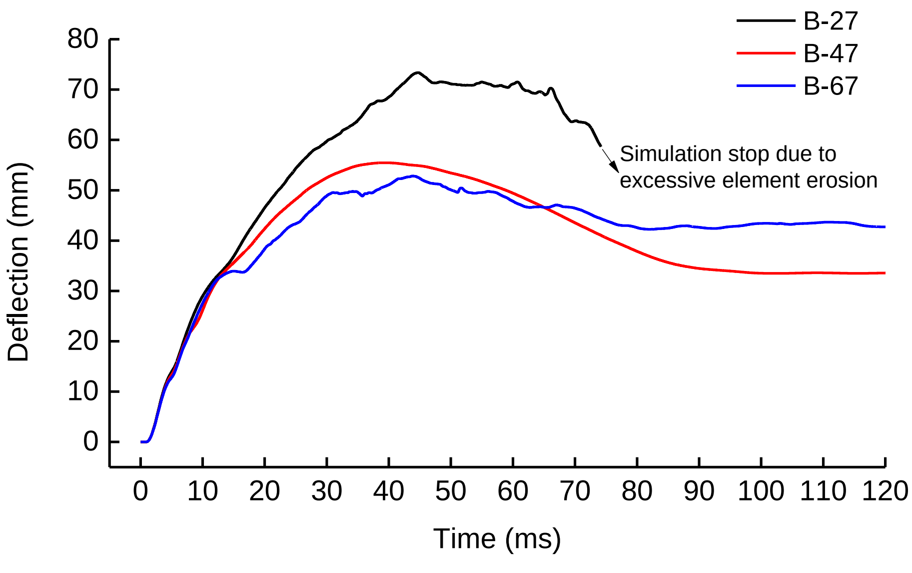

(b)

Fig. 20 Numerical results of beams with different GPC compressive strengths: (a) effective plastic strain contours and (b) midspan deflection time histories

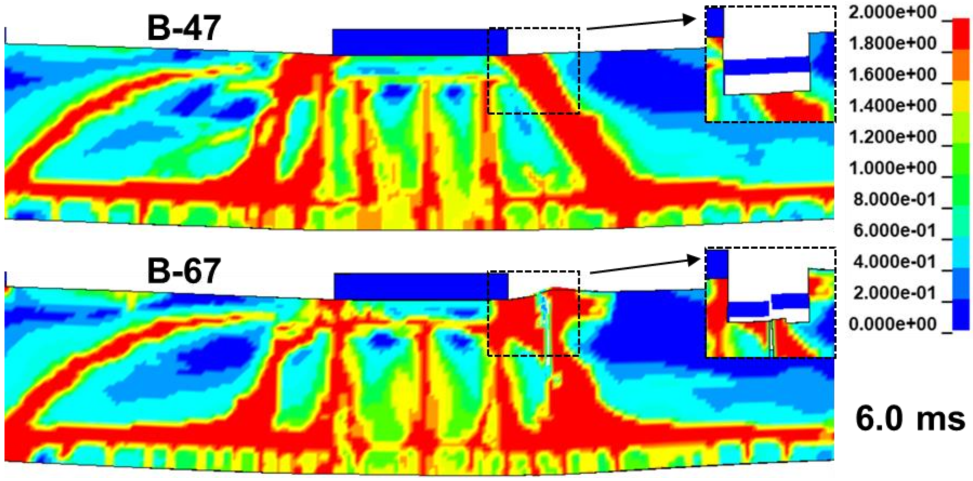

Fig. 21 Effective plastic strain contours of Beams B-47 and B-67 at 6.0 ms

6.2. Effect of tension reinforcement ratio

Beside concrete compressive strength, the shear resistance contributed by concrete is influenced by tension reinforcement ratio (contributed by dowel action and aggregate interlocking) [21]. Therefore, four beams, i.e. B-T-1.2%, B-T-1.6%, B-T-2.5%, and B-T-3.6% (‘T’ denotes tension reinforcement), with tension reinforcement ratios of 1.2%, 1.6%, 2.5%, and 3.6%, respectively, were modelled by changing the diameter of tension reinforcements (the corresponding diameters: 14 mm, 16 mm, 20 mm, and 24 mm), while keeping all the other parameters unchanged. **Fig. 22** shows the numerical results in terms of effective plastic strain contour and midspan deflection time history. As can be seen, increasing the tension reinforcement ratio, the beam experienced less severe concrete damage and lower maximum and residual deflection. However, further increasing the tension reinforcement ratio up to 3.6% barely decreased the residual deflection, with the converged residual deflection of about 24.5 mm.

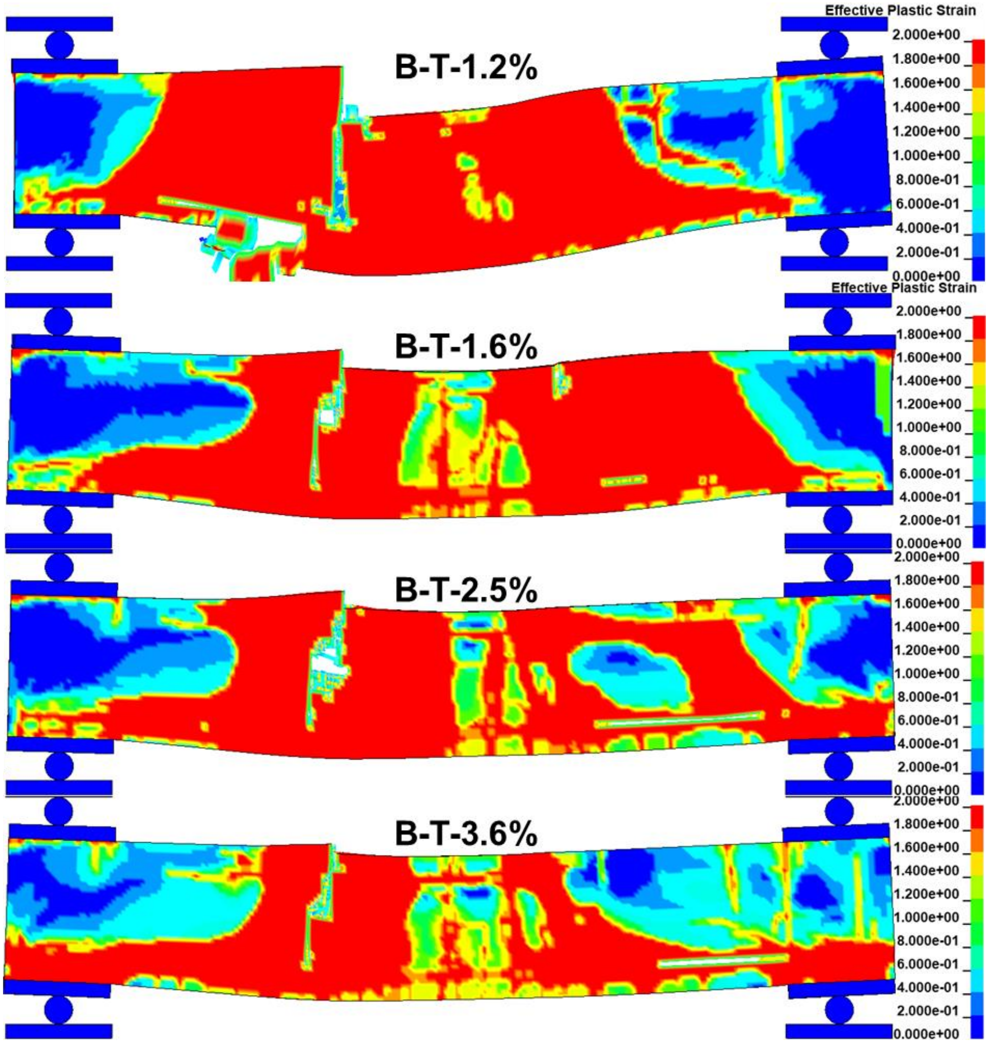

532 (a)

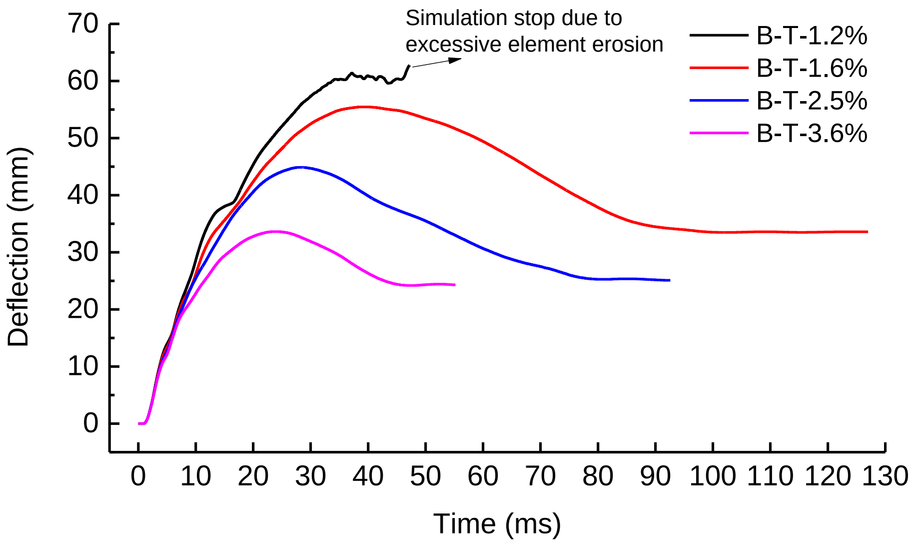

533 (b)

534 **Fig. 22** Numerical results of beams with different tension reinforcement ratios: (a) effective plastic
535 strain contours and (b) midspan deflection time histories

6.3. Effect of stirrup ratio

Shear resistance of the beam is affected by stirrups. Stirrup ratios of 0.17%, 0.26%, and 0.38% were adopted for three beams, i.e., B-S-0.17%, B-S-0.26%, and B-S-0.38% ('S' denotes stirrup), with diameters of 4 mm, 5 mm, and 6 mm, respectively. **Fig. 23** shows the effective plastic strain contours of the beams with different stirrup ratios and their corresponding midspan deflection time histories. With the increasing stirrup ratio, the beams had lower effective plastic strain and decreasing maximum midspan deflection (i.e. 55.5 mm, 45.9 mm, and 34.9 mm), indicating less damage to the beams under impact loads. It was also observed that increasing the stirrup ratio from 0.17% to 0.26% barely decreased the residual deflection, because the residual deflection is strongly influenced by the splitting damage of the top longitudinal bars of Beams B-S-0.17% and B-S-0.26% on two sides. When the stirrup ratio increased to 0.38%, only one side of Beam B-S-0.38% experienced splitting damage of the top longitudinal bars and the residual deflection decreased greatly from 33.6 mm to 10.1 mm. Therefore, it is concluded that using sufficient stirrup ratio can significantly improve the impact resistance of the beams and simultaneously reduce their residual deflection.

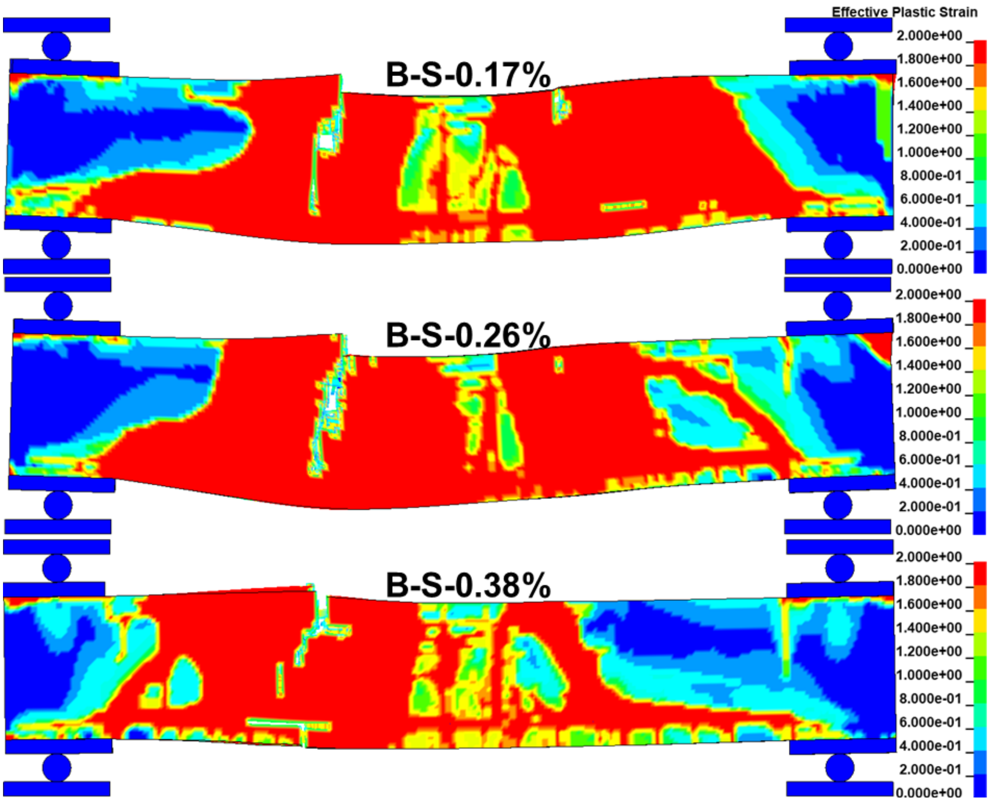

(a)

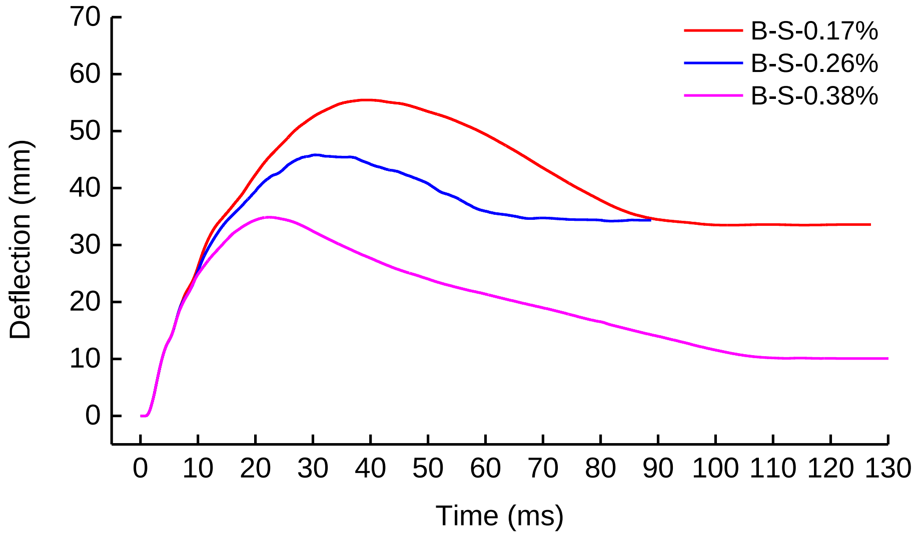

(b)

Fig. 23 Numerical results of beams with different stirrup ratios: (a) effective plastic strain contours and (b) midspan deflection time histories

6.4. Effect of compression reinforcement type

Splitting damage of compression FRP reinforcements was observed under impact loads due to large transverse shear force. It is well known that FRP bars are strong in tension but relatively weak in shear and compression. In this section, the effect of compression reinforcement type was investigated by replacing the top longitudinal BFRP bars with the same-diameter (16mm) steel bars based on the design of Beam GPC-I-RS-47. The GPC strength was 47 MPa and the longitudinal and transverse reinforcement ratios were 1.60% and 0.17%, respectively. The steel reinforcements with yield strength of 500 MPa (density 7800 kg/m^3, modulus of elasticity 200 GPa, Poisson's ratio 0.3, tangent modulus 2 GPa, and failure strain 0.15 [71]) and the BFPR bars were used as compression reinforcements for Beams B-C-Steel and B-C-BFRP ('C' means compression reinforcement), respectively. **Fig. 24** shows the predicted failure modes and the midspan deflection time histories of the two beams. As shown, Beam B-C-Steel experienced less severe concrete damage and splitting damage of compression reinforcements than Beam B-C-BFRP. The maximum deflection of Beams B-C-BFRP and B-C-Steel was 55.5 mm and 31.2 mm, respectively, and their residual deflection was 33.6 mm and 28.5 mm, respectively. It should be noted that the residual deflection of Beam B-C-Steel recovered only slightly from the maximum deflection, which was due to reaching yielding strength of steel reinforcements.

Therefore, the use of steel bars as compression reinforcement could mitigate possible splitting damage of BFRP reinforcements for concrete beams subjected to impact loads.

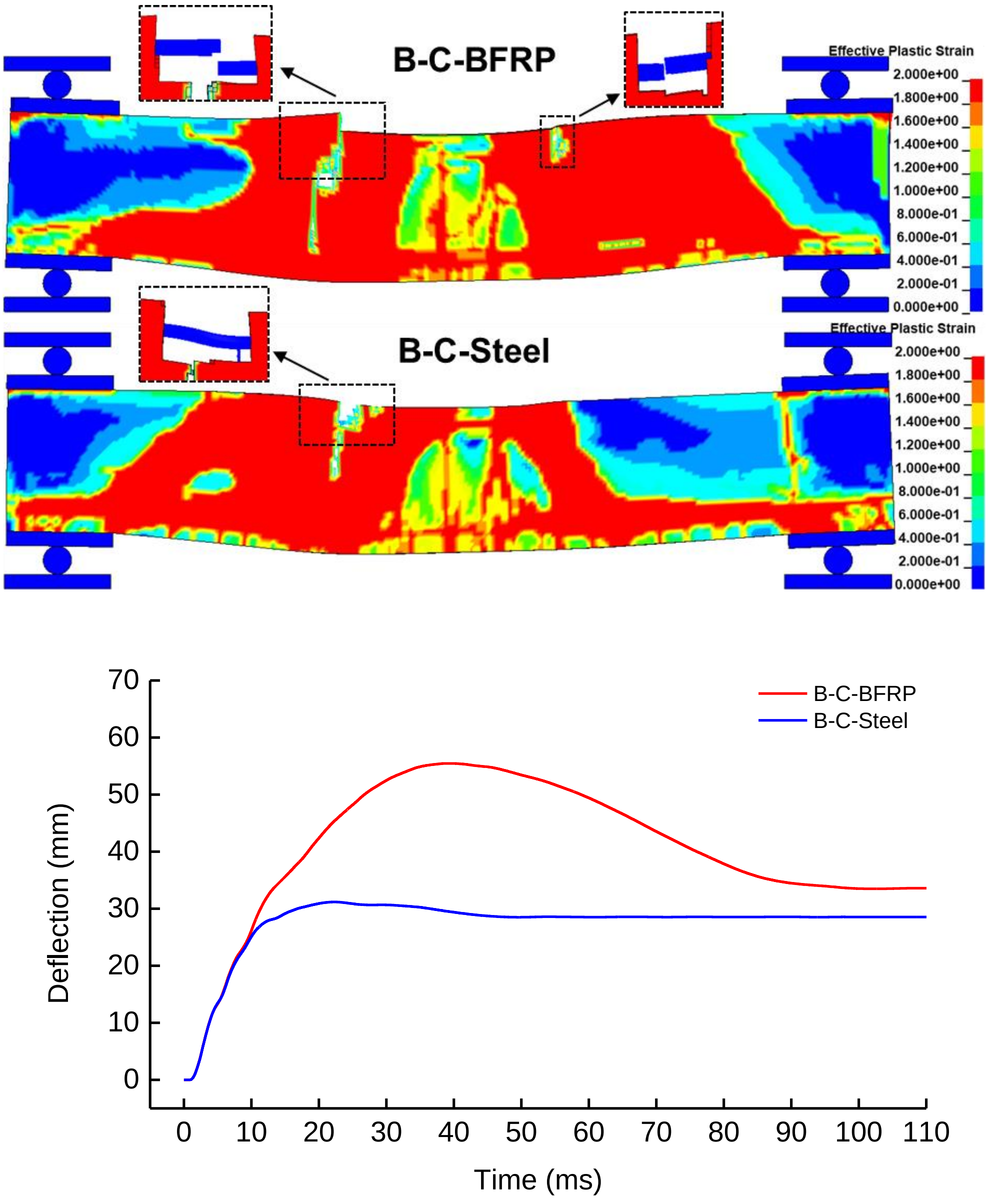

(a)

(b)

Fig. 24 Numerical results of beams with different compression reinforcement type: (a) effective plastic strain contours and (b) midspan deflection time histories

7. Conclusion

This study investigated the shear behaviour of GPC beams reinforced with BFRP bars under static and impact loads. Based on the test and numerical results, the following conclusions are drawn:

1. The beams under static loads failed in shear by diagonal tension as expected. The normalized load-midspan deflection curves of the beams exhibited bilinear behaviour, i.e., a steep linear portion representing the uncracked stage and a reduced-slope portion until the failure of the beams.

2. The shear capacities of the GPC beams reinforced with BFPR bars under static loads could be well predicted by Standard CSA S806-12 [18] with the average ratio of prediction to testing results of 0.94 whereas Standard ACI 440.1R-15 [19] gave more conservative prediction with the average ratio of 0.61. This could be because ACI 440.1R-15 [19] usually gives more conservative prediction by considering the effect of axial stiffness of tension BFRP bars on the shear contribution of concrete as compared to CSA S806-12 [18].

3. The GPC beams reinforced with BFRP bars under impact loads experienced severer concrete damage and splitting damage of top longitudinal BFRP bars, but less flexural cracks as compared to those under static loads. The splitting damage of top longitudinal BFRP bars under impact loads could lead to severer concrete damage and large midspan deflection of beams.

4. As compared to rectangular stirrups, spiral stirrups with the same stirrup ratio demonstrated superior performance and led to higher normalized shear capacity of the beams under static loads and smaller maximum and residual deflection of the beams under impact loads, which is attributed to the longitudinal confinement provided by the spiral stirrups.

5. The GPC material could be simulated in LS-DYNA by using KCC model with the modified parameters based on GPC material test data. The numerical predictions of the behaviours of the GPC beams reinforced with BFRP bars were in good agreement with the test results.

6. Numerical simulation indicated that decreasing the GPC compressive strength from 47 MPa to 27 MPa could result in severer damage of the beam. Increasing the GPC compressive strength from 47 MPa to 67 MPa was not necessarily beneficial to the impact resistance of the beam as it could lead to more concentrated concrete damage, resulting in severer splitting damage of compression BFRP bars, and larger residual deflection.

7. Increasing the tension reinforcement ratio and stirrup ratio could effectively reduce the concrete damage level and the midspan deflection of the beam. The use of steel bars as compression reinforcement of GPC beams could mitigate possible splitting damage of BFRP reinforcements subjected to impact loads because of the higher compression and shear strength of steel bars.

8. Acknowledgements

The authors acknowledge the financial support from the Australian Research Council (ARC) via Australian Laureate Fellowship (FL180100196).

9. References

[1] Dadsetan S, Siad H, Lachemi M, Sahmaran M. Construction and demolition waste in geopolymer concrete technology: a review. Mag Concr Res. 2019;71:1232-52.

[2] Hardjito D, Rangan BV. Development and properties of low-calcium fly ash-based geopolymer concrete. Perth, Australia: Faculty of Engineering, Curtin University of Technology; 2005.

[3] Mahmoodi O, Siad H, Lachemi M, Dadsetan S, Sahmaran M. Optimization of brick waste-based geopolymer binders at ambient temperature and pre-targeted chemical parameters. J Cleaner Prod. 2020;268.

[4] Mahmoodi O, Siad H, Lachemi M, Dadsetan S, Sahmaran M. Development of ceramic tile waste geopolymer binders based on pre-targeted chemical ratios and ambient curing. Constr Build Mater. 2020;258.

[5] Singh B, Ishwarya G, Gupta M, Bhattacharyya SK. Geopolymer concrete: A review of some recent developments. Constr Build Mater. 2015;85:78-90.

[6] Tang Z, Li W, Tam VWY, Yan L. Mechanical performance of CFRP-confined sustainable geopolymeric recycled concrete under axial compression. Eng Struct. 2020;224.

[7] Tang Z, Li W, Tam VWY, Yan L. Mechanical behaviors of CFRP-confined sustainable geopolymeric recycled aggregate concrete under both static and cyclic compressions. Compos Struct. 2020;252.

[8] Huang Z, Chen W, Hao H, Chen Z, Pham TM, Tran TT, et al. Flexural Behaviour of Ambient Cured Geopolymer Concrete Beams Reinforced with BFRP Bars under Static and Impact Loads. Compos Struct. 2020;(accepted).

[9] GangaRao HV, Taly N, Vijay P. Reinforced concrete design with FRP composites. Boca Raton, Florida: CRC press, 2006.

[10] Maranan GB, Manalo AC, Benmokrane B, Karunasena W, Mendis P, Nguyen TQ. Shear behaviour of geopolymer-concrete beams transversely reinforced with continuous rectangular GFRP composite spirals. Compos Struct. 2018;187:454-65.

[11] Ahmed HQ, Jaf DK, Yaseen SA. Flexural strength and failure of geopolymer concrete beams reinforced with carbon fibre-reinforced polymer bars. Constr Build Mater. 2020;231:117185.

[12] Tureyen AK, Frosch RJ. Shear tests of FRP-reinforced concrete beams without stirrups. ACI Struct J. 2002;99:427-34.

[13] Guadagnini M, Pilakoutas K, Waldron P. Shear resistance of FRP RC beams: Experimental study. J Compos Constr. 2006;10:464-73.

[14] Bentz EC, Massam L, Collins MP. Shear strength of large concrete members with FRP reinforcement. J Compos Constr. 2010;14:637-46.

[15] Farghaly AS, Benmokrane B. Shear behavior of FRP-reinforced concrete deep beams without web reinforcement. J Compos Constr. 2013;17:04013015.

[16] Razaqpur AG, Spadea S. Shear Strength of FRP Reinforced Concrete Members with Stirrups. J Compos Constr. 2015;19.

[17] Chen H, Yi W-J, Ma ZJ, Hwang H-J. Modeling of shear mechanisms and strength of concrete deep beams reinforced with FRP bars. Compos Struct. 2020;234:111715.

[18] CSA S806-12. Design and construction of building structures with fibre-reinforced polymers. Ontario, Canada: Canadian Standards Association; 2012.

[19] ACI 440.1R-15. Guide for the design and construction of concrete reinforced with Fiber Rienforced Polymers (FRP) bars. Farmington Hills, MI, USA: American Concrete Institute; 2015.

[20] Maranan GB, Manalo AC, Benmokrane B, Karunasena W, Mendis P. Shear Behavior of Geopolymer Concrete Beams Reinforced with GFRP Bars. ACI Struct J. 2017;114.

[21] Wight JK. Reinforced Concrete: Mechanics and Design (Seventh Edition). 7th ed. New Jersey, USA: Pearson Education, Inc., 2015.

[22] Goldston M, Remennikov A, Sheikh MN. Experimental investigation of the behaviour of concrete beams reinforced with GFRP bars under static and impact loading. Eng Struct. 2016;113:220-32.

[23] Goldston MW, Remennikov A, Saleh Z, Sheikh MN. Experimental investigations on the behavior of GFRP bar reinforced HSC and UHSC beams under static and impact loading. Structures. 2019;22:109-23.

[24] Saleh Z, Sheikh MN, Remennikov A, Basu A. Numerical Analysis of Behavior of Glass Fiber-Reinforced Polymer Bar-Reinforced Concrete Beams under Impact Loads. ACI Struct J. 2019;116:151-60.

[25] Saleh Z, Sheikh MN, Remennikov A, Basu A. Overload Damage Mechanisms of GFRP-RC Beams Subjected to High-intensity Low-velocity Impact Loads. Compos Struct. 2019:111578.

[26] Saleh Z, Sheikh MN, Remennikov A, Basu A. Damage assessment of GFRP bar reinforced ultra-high-strength concrete beams under overloading impact conditions. Eng Struct. 2020;213:110581.

[27] Thomas RJ, Peethamparan S. Alkali-activated concrete: Engineering properties and stress–strain behavior. Constr Build Mater. 2015;93:49-56.

[28] Farhan NA, Sheikh MN, Hadi MN. Investigation of engineering properties of normal and high strength fly ash based geopolymer and alkali-activated slag concrete compared to ordinary Portland cement concrete. Constr Build Mater. 2019;196:26-42.

[29] Nath P, Sarker PK. Effect of GGBFS on setting, workability and early strength properties of fly ash geopolymer concrete cured in ambient condition. Constr Build Mater. 2014;66:163-71.

[30] Khan MZN, Hao Y, Hao H. Synthesis of high strength ambient cured geopolymer composite by using low calcium fly ash. Constr Build Mater. 2016;125:809-20.

[31] Tran TT, Pham TM, Hao H. Experimental and analytical investigation on flexural behaviour of ambient cured geopolymer concrete beams reinforced with steel fibers. Eng Struct. 2019;200:109707.

[32] Jiangsu Green Materials Vally New Material T&D Co. Ltd (GMV). Basalt Fiber Composite Bar. China.

[33] Banyhussan QS, Yıldırım G, Anıl Ö, Erdem RT, Ashour A, Şahmaran M. Impact resistance of deflection‐hardening fiber reinforced concretes with different mixture parameters. Struct Concr. 2019;20:1036-50.

[34] Yıldırım G, Khiavi FE, Anıl Ö, Şahin O, Şahmaran M, Erdem RT. Performance of engineered cementitious composites under drop‐weight impact: Effect of different mixture parameters. Struct Concr. 2019;21:1051-70.

[35] Pham TM, Hao H. Impact Behavior of FRP-Strengthened RC Beams without Stirrups. J Compos Constr. 2016;20.

[36] El-Sayed AK, El-Salakawy EF, Benmokrane B. Shear strength of FRP-reinforced concrete beams without transverse reinforcement. ACI Struct J. 2006;103:235.

[37] Alam MS, Hussein A. Unified shear design equation for concrete members reinforced with fiber-reinforced polymer without stirrups. J Compos Constr. 2012;17:575-83.

[38] Tomlinson D, Fam A. Performance of concrete beams reinforced with basalt FRP for flexure and shear. J Compos Constr. 2014;19:04014036.

[39] El Refai A, Abed F. Concrete contribution to shear strength of beams reinforced with basalt fiber-reinforced bars. J Compos Constr. 2015;20:04015082.

[40] El-Sayed AK, Soudki K. Evaluation of shear design equations of concrete beams with FRP reinforcement. J Compos Constr. 2010;15:9-20.

[41] Kim CH, Jang HS. Concrete shear strength of normal and lightweight concrete beams reinforced with FRP bars. J Compos Constr. 2013;18:04013038.

[42] fib. Bulletin 40. FRP reinforcement in RC structures. Lausanne, Switzerland: International Federation for Structural Concrete (fib); 2007.

[43] Li HW, Chen WS, Hao H. Factors influencing impact force profile and measurement accuracy in drop weight impact tests. Int J Impact Eng. 2020;145:103688.

[44] LSTC. LS-DYNA Theory Manual. Livermore, California, USA: Livermore Software Technology Corporation; 2019.

[45] LSTC. LS-DYNA Keyword User's Munual Volume II: Material Models. Livermore, California, USA: Livermore Software Technology Corporation; 2019.

[46] Tran TT, Pham TM, Hao H. Rectangular Stress-block Parameters for Fly-ash and Slag Based Geopolymer Concrete. Structures: Elsevier; 2019. p. 143-55.

[47] Liu J, Wu C, Chen X. Numerical study of ultra-high performance concrete under non-deformable projectile penetration. Constr Build Mater. 2017;135:447-58.

[48] Mao L, Barnett S, Begg D, Schleyer G, Wight G. Numerical simulation of ultra high performance fibre reinforced concrete panel subjected to blast loading. Int J Impact Eng. 2014;64:91-100.

[49] Malvar LJ, Crawford JE, Wesevich JW, Simons D. A plasticity concrete material model for DYNA3D. Int J Impact Eng. 1997;19:847-73.

[50] Shi Y, Hao H, Li Z-X. Numerical derivation of pressure–impulse diagrams for prediction of RC column damage to blast loads. Int J Impact Eng. 2008;35:1213-27.

[51] Chen WS, Hao H, Chen SY. Numerical analysis of prestressed reinforced concrete beam subjected to blast loading. Mater Des. 2015;65:662-74.

[52] Li J, Hao H, Wu C. Numerical study of precast segmental column under blast loads. Eng Struct. 2017;134:125-37.

[53] Li H, Chen W, Hao H. Dynamic response of precast concrete beam with wet connection subjected to impact loads. Eng Struct. 2019;191:247-63.

[54] Australia Standard. Methods of testing concrete – Method 9: Compressive strength tests -Concrete, mortar and grout specimens. Sydney, NSW, Australia: Standards Australia Limited; 2014.

[55] Li J, Zhang Y. Evolution and calibration of a numerical model for modelling of hybrid-fibre ECC panels under high-velocity impact. Compos Struct. 2011;93:2714-22.

[56] ACI 318-14. Building Code Requirements for Structural Concrete (ACI 318-14) and Commentary on Building Code Requirements for Structural Concrete (ACI 318-14). Farmington Hills, MI, USA: American Concrete Institute; 2014.

[57] Chen W, Hao H, Jong M, Cui J, Shi Y, Chen L, et al. Quasi-static and dynamic tensile properties of basalt fibre reinforced polymer. Compos Part B-Eng. 2017;125:123-33.

[58] Malvar LJ. Review of static and dynamic properties of steel reinforcing bars. ACI Mater J. 1998;95:609-16.

[59] Feng KN, Ruan D, Pan Z, Collins F, Bai Y, Wang CM, et al. Effect of strain rate on splitting tensile strength of geopolymer concrete. Mag Concr Res. 2014;66:825-35.

[60] Feng KN, Ruan D, Pan Z, Collins F, Bai Y, Wang CM, et al. Mechanical behavior of geopolymer concrete subjected to high strain rate compressive loadings. Mater Struct. 2015;48:671-81.

[61] Li H, Chen W, Hao H. Influence of drop weight geometry and interlayer on impact behavior of RC beams. Int J Impact Eng. 2019;131:222-37.

[62] Almusallam TH, Elsanadedy HM, Al-Salloum YA, Alsayed SH. Experimental and numerical investigation for the flexural strengthening of RC beams using near-surface mounted steel or GFRP bars. Constr Build Mater. 2013;40:145-61.

[63] Abdollahi A. Numerical strategies in the application of the FEM to RC structures—I. Computers & structures. 1996;58:1171-82.

[64] Tonge AL, Ramesh K. Multi-scale defect interactions in high-rate failure of brittle materials, Part II: application to design of protection materials. J Mech Phys Solids. 2016;86:237-58.

[65] Tonge AL, Ramesh K. Multi-scale defect interactions in high-rate brittle material failure. Part I: model formulation and application to ALON. J Mech Phys Solids. 2016;86:117-49.

[66] Meng Q, Wu C, Su Y, Li J, Liu J, Pang J. A study of steel wire mesh reinforced high performance geopolymer concrete slabs under blast loading. J Cleaner Prod. 2018.

[67] Pham TM, Hao H. Plastic hinges and inertia forces in RC beams under impact loads. Int J Impact Eng. 2017;103:1-11.

[68] Farnam Y, Mohammadi S, Shekarchi M. Experimental and numerical investigations of low velocity impact behavior of high-performance fiber-reinforced cement based composite. Int J Impact Eng. 2010;37:220-9.

[69] Li J, Hao H. Numerical study of concrete spall damage to blast loads. Int J Impact Eng. 2014;68:41-55.

[70] Dong Z, Keru W. Fracture properties of high-strength concrete. J Mater Civ Eng. 2001;13:86-8.

[71] Pham TM, Hao Y, Hao H. Sensitivity of impact behaviour of RC beams to contact stiffness. Int J Impact Eng. 2018;112:155-64.